ically expressed in dopaminergic neurons and was confirmed to be present in the current MSC-DP cells in vitro. The high uptake of ^{11}C-CFT was not found in any of the sham-operated animals, even though they received PBS injections, which may induce tissue damage or inflammation. Third, the study does not clarify the complete mechanism underlying the motor recovery in the current animals. PET findings revealed increased DAT expression only in the early phase, while behavioral data showed significant recovery only in the later phase. As described above, we believe the discrepancy is explained by a time delay required for the remaining MCS-DP cells to achieve synaptic connections with the host tissues. This speculation should be clarified in the future study, since the delayed motor recovery found here seems to be common in trials of cell replacement therapies in PD. For example, fetal tissue grafting improved motor symptoms at 6 to 9 months after grafting in selected patients with PD (39). ES cell–derived well-differentiated DA neurons also restored motor behaviors 3–5 months after grafting in an animal model (47). Finally, these data do not show convincing evidence that benefits were truly results of an in vitro process differentiating MSCs into A9 DA neurons. We cannot completely exclude the possibility that undifferentiated MSCs, contaminated in the graft and not positive for A9 markers (25%–50% of cells; Figure 1K), might have contributed to the observed benefits, for example, by way of trophic effects. Therefore, future studies should directly compare the MSC-DP cell with naive MSC transplantation.

In conclusion, this study indicates that the autologous MSC-differentiation system may be safe and potentially effective for restoring motor dysfunction in hemiparkinsonian nonhuman primate animals. Although further studies are needed to improve the viability of MSC-DP cells and net performance for functional recovery, the current system may expand the availability of cell sources for cell-based therapies for patients with PD.

Methods

Ten adult male cynomolgus monkeys (*Macaca fascicularis*; body weight, 3–4 kg) were used in this study. All animals were housed in a room kept at 26°C. Animals were pretreated with the neurotoxin MPTP to generate a hemiparkinsonian model, and their bone marrow aspirates were used for induction of autologous MSC-DP cells. Five animals were used for the engraftment of MSC-PD cells (n = 5, MSC-DP group), and the remaining 5 underwent a sham operation in which they received injection of PBS only (n = 5, sham group).

Isolation of MSCs from bone marrow aspirates. Primary MSCs were isolated from bone marrow aspirates obtained from the iliac bone of every animal in the engrafted group. Bone marrow was aspirated from each animal 3–4 months prior to transplantation under deep anesthesia achieved by intramuscular injection of ketamine (6.6 mg/kg), xylazine (1.3 mg/kg), and atropine (0.01 mg/kg). For aspiration, we used a bone marrow needle (18 G; Sheen-man Co. Ltd.) and 2.5-ml aspiration syringes containing 100 units of heparin (Novo-Heparin, Mochida Pharmaceutical Co. Ltd.) to prevent clotting. Aspirates were diluted 1:10 using culture medium (α-minimum essential medium [α-MEM] plus 15% FBS plus 2 mM L-glutamine plus kanamycin) and incubated at 37°C in 5% CO_2. After 4 days, nonadherent cells were removed by replacing the medium. Adherent cells, namely, MSCs, were subjected to subculture when they reached 95% confluence and were subcultured 4 times. Finally, they were subjected to dopaminergic neuronal differentiation.

Differentiation of MSC-DP cells from MSCs. MSC-DP cells were differentiated from MSCs using a method of spermine-pullulan–mediated reverse transfection, as described previously (21). We used pullulan, with an average molecular weight of 47,300 Da (Hayashibara Biochemical Laboratories) and spermine (Sigma-Aldrich). A cationized pullulan derivative was prepared as described previously (21), and a gene encoding mouse NICD (constitutively active form), including a transmembrane region with a small fragment of extracellular domain and the entire intracellular domain, was subcloned into the pCI-neo vector (Promega) (pCI-NICD). Cells were further selected by G418 for 3 to 4 days, replated at a cell density of 2,080 cells per cm^2, and treated with 5 μM forskolin (Calbiochem), 10 ng/ml bFGF (Peprotech), and 10 ng/ml CNTF (R&D Systems) in α-MEM containing 5% FBS for 5 days. Finally, GDNF (50 ng/ml; Peprotech) was added.

Evaluation of MSC-DP cells — dopamine release assay using HPLC. The dopamine release assay was performed as described previously (20, 21). Briefly, cells were washed in a low K^+ solution for 5 minutes, and the medium was replaced with a high K^+ solution for 5 minutes. The concentration of released dopamine was determined using HPLC with a reverse-phase column and an electrochemical detector system (Eicom Corporation). The mobile phase was composed of 0.1 M phosphate buffer (pH 6.0), 20% methanol. The amount of dopamine release was measured according to the number of cells, which were counted after trypsinization.

Evaluation of MSC-DP cells — immunocytochemistry. The primary antibodies used were anti-MAP-2ab (1:250; Sigma-Aldrich) and anti-Tuj1 (1:100; BAbCO) as neuron-specific markers and anti-TH (1:1,000; Chemicon, Millipore), anti-DAT (1:100; Millipore), anti-GIRK2 (1:80; Alomone Labs), and anti-FOXA2 (1:50; Santa Cruz Biotechnology Inc.) as markers of dopaminergic neurons. We also used an anti–sodium channel antibody (PAN) (clone K58/35, 1:1,000; Sigma-Aldrich) as a marker of neurons. Secondary antibodies were anti-mouse or anti-rabbit IgG antibodies conjugated to Alexa Fluor 488 (Invitrogen) and anti-rabbit or anti-goat IgG conjugated to Cy3 (Jackson ImmunoResearch Laboratory). Nuclei were counterstained with DAPI and inspected using confocal laser microscopy (Nikon Corporation).

Evaluation of MSC-DP cells — RT-PCR. We analyzed the relative expression levels of *GIRK2*, *FOXA2*, and *CALB1* mRNAs using RT-PCR to classify MSC-DP cells as A9-type neurons (*GIRK2*$^+$/*FOXA2*$^+$/*CALB1*$^-$) or A10-type neurons (*GIRK2*$^-$/*FOXA2*$^-$/*CALB1*$^+$) (28, 29, 56). The amount of cDNA was normalized on the basis of the signal from the ubiquitously expressed β-actin. The primers were designed based on the cDNA sequence of the *Macaca mulatta*, which is highly homologous to that of *Rattus norvegicus*, as revealed by an alignment search tool (BLAST; http://www.ncbi.nlm.nih.gov/BLAST/). The primer sequences and precise conditions were as follows: β-actin, 5′-TCTAGGCGGACTGTGACTTACTTGCGTTAC-3′ (forward) and 5′-AATCAAAGTCCTCGGCCACATTGTAGAACT-3′ (reverse) (TM, melting temperature; 60°C, 25 cycles); GIRK2, 5′-ATCCAGAGGTATGTGAGGAAAGATG-3′ (forward) and 5′-CACTGTGTAAACCATGACGAAAATC-3′ (reverse) (TM, melting temperature; 55°C, 40 cycles); calbindin, 5′-GCTGTATGATCAGGACGGCAAT-3′ (forward) and 5′-TCTAGTTATCCCCAGCACAGAGAA-3′ (reverse) (TM, melting temperature; 58°C, 40 cycles); and FOXA2, 5′-CGGTGTTGCAGAGACGAAAG-3′ (forward) and 5′-CAGAATCTGCAGGTGCTTGAAG-3′ (reverse) (TM, melting temperature; 58°C, 40 cycles). As a positive control for GIRK2, FOXA2, and calbindin, total RNA was collected and analyzed using 2 types of brain tissues from cynomolgus embryos (~6th fetal month, *Macaca fascicularis*) and an adult animal (8 years old, *Macaca fascicularis*), namely, the SNc and VTA.

MPTP-induced hemiparkinsonism. The animal model of the unilateral PD was produced using the neurotoxin MPTP, as previously reported (30, 57), with some modifications. Briefly, animals received slow arterial injections of MPTP into the right carotid artery. Unlike previous studies that accessed the carotid artery by incision of the upper cervical area, we

applied an angiographic approach that allowed us to access the target artery less invasively and did not require postoperative occlusion of the target artery, which causes insufficient cerebral circulation. We used an 80-cm-long catheter (3F, CATEX Co. Ltd.) and X-ray angiographic device (OEC 8800, GE Healthcare) to place the catheter into the internal carotid artery. After the tip of the catheter was placed in the proximal (cervical) portion of the internal carotid artery, the MPTP solution (0.4 mg/kg dissolved in 40 ml of saline, pH 7.4) was infused at a rate of 2 ml per minutes. In every animal, the right pupil showed dilatation with a diameter >5 mm, indicating the adrenergic effect of MPTP (58). All animals recovered safely from anesthesia and exhibited hemiparkinsonism with a crooked arm posture and dragging leg, with slow or disabled movements in the left hand and arm. All animals continuously revealed hemiparkinsonism over a period of 3 months, and none of them showed spontaneous recovery from motor disabilities.

Engrafting MSC-DP cells into the striatum. Under deep anesthesia, each animal in the engraftment group underwent MRI-guided stereotactic surgery for engrafting of MSC-DP cells into the putamen on the right side (the same side as the MPTP infusion). The animal's head was fixed to a stereotactic acrylic holder in a sphinx position, the head skin and muscles were incised under aseptic conditions after subcutaneous injection of lidocaine (Xylocain 2%, AstraZeneca PLC), and the surface of the cranium bone was exposed by separating the galea aponeurotica. Three to four MRI-visible markers were attached to the fringe of the exposed cranium to be used as a reference for co-registering the translocation between MRI and the stereotactic micromanipulator. Then, the stereotactic holder was placed horizontally on the MRI gantry with its axis parallel to the *z* axis of the MRI bore, and a high-resolution head MRI scan was obtained with the inversion recovery-fast spoiled gradient recalled echo (IR-FSPGR) sequence. Obtained MRI images were transformed with a 3D translocation algorithm to the standard macaque brain template (31) and resliced in a volume with a matrix of 110,134,80 voxels, a cubic voxel size of 0.5-mm edge length, and an origin at the midportion of the anterior commissure (AC). On 3 coronal views of the MRI image sectioned at AC −5, −7, and −9 mm, we determined 12 target points for transplantation (Figure 3A). For each of the 12 targets, the relative coordinates were read on the MRI image in reference to one of the markers on the cranium. After MRI scans were finished, the head holder was then attached to a customized metallic stereotaxic apparatus on which the stereotactic coordinates of the markers were read using a micromanipulator (SM-15 Narishige Group). Then the target coordinates in the micromanipulator were determined based on the coordinates of the reference markers in the MRI image and their location relative to that of the micromanipulator.

Immediately before injecting cells, the autologous MSC-DP cells were collected and suspended in 60 μl of 0.1 M PBS, and the number of cells was counted. The average total cell count was $14.0 \times 10^6 \pm 5.0 \times 10^6$ (mean ± SD), with a range of 9.0×10^6 to 20.4×10^6 (Table 1). For each target coordinate of *x* and *y* determined by above method, the tip of a 10-μl Hamilton syringe with a 30-gauge needle was slowly advanced vertically and kept in place at the target coordinate for *z*. Then MSC-DP cells in PBS solution were injected at a rate of 0.5 μl per minute until a total of 5 μl had been injected at each target site. The needle was kept in place for an additional 3 minutes to allow the injectate to diffuse and then slowly retracted to minimize diffusion of the injectate over the cortical surface. The sham operation group received injection of the same amount of PBS solution in the same 12 target points in the right dorsal posterior putamen.

Behavioral analysis of motor function. Behavioral performance was assessed using the CRSs, hand-reach scores for the affected hands, and spontaneous activities in housing cages. The previously validated CRSs were used to quantitatively assess the parkinsonian status of the monkeys (59, 60). The scale consists of ratings of posture (0 to 2), gait (0 to 5), bradykinesia (0 to 5), balance (0 to 2), tremor for each arm (0 to 3), gross motor skills (0 to 4 for each arm), defense reaction (0 to 2), and freezing (0 to 2). The score was the sum of the features out of a total of 32 points, with 0 corresponding to normal and 32 corresponding to severe disability. Scores were assessed before and 14 days, 2 months, 4 months, and 8 months after engrafting and were evaluated by an experimenter blinded to the group allocation.

Hand-reach scores were assessed based on food-taking behavior by the affected hand, as described previously (30, 61), and were assessed at the same time points as CRSs (before and 14 days, 2 months, 4 months, and 8 months after engraftment). Five ~5-mm^3 pieces of apple were placed in front of a circular hole (6-cm diameter) in the lower corner of the cage, so that the animals could pick up the pieces and eat them. Five trials were performed for each session, and three sessions were performed on each of three consecutive days at each time point. Evaluations were made before engrafting and 14 days, 2 months, 4 months, and 8 months after engrafting. All behaviors during the task were monitored and recorded by video. After collection of all data, an experimenter blinded to the group allocation of animals scored the movement velocity of the proximal forelimb (arm and forearm) on a scale of 0 to 5 (0 means very fast, 5 means very slow), the movement velocity of hand grasping and finger pinching on a scale of 0 to 4, and the accuracy of food picking on a scale of 0 to 2. The sum of these items was recorded as the hand-reach score, with 11 corresponding to normal and 0 corresponding to severe disability.

We also measured spontaneous body activities by monitoring movements using a passive infrared system for monitoring spontaneous animal activities (Supermex, Muromachi Kikai Co. Ltd.) before and 14 days, 4 months and 8 months after engraftment. The animals were placed in a 600-mm-wide × 700-mm-deep × 740-mm-high cage, in which they were housed for acclimation beforehand. Activities were monitored consecutively for a period of 3 days (72 hours). The infrared sensor was attached so as to cover the whole cage in a single field of view. Data were imported to a computer and analyzed using a dedicated program for counting the number of pixels showing signal changes in a 10-minute time frame.

PET. We performed ^{11}C-CFT PET scanning to evaluate DAT expression in cynomolgus brains, as described previously (26, 62). The tracer ^{11}C-CFT was prepared by a conventional method using ^{11}C-methyl-triflate (63) and a precursor, nor[methyl-^{11}C]2-β-carbomethoxy-3-β-(4-fluorophenyl)tropane. The animals received intramuscular injections of ketamine and xyladine, followed by continuous intravenous infusion of propofol (6 mg/kg/h) to achieve anesthesia, and their respiration was assisted using an anesthetic machine (Cato, Drager) with an inspired gas mixture of O_2 and N_2 (O_2/N_2 = 30%:70%). We monitored endotidal CO_2 level ($EtCO_2$) and percutaneous oxygen saturation level (SpO_2), and, if needed, adjusted the respiration rate to achieve SpO_2 >95% and $EtCO_2$ of 35 mmHg. After achieving deep anesthesia, animals were placed on the PET gantry, and their bodies were kept warm by using a temperature managing unit (Bair Hugger Model 505, Arizant Inc.). A 15-minute transmission scan was obtained using a 68Ge/68Ga rod source for attenuation correction; then, 187 MBq of [^{11}C]-CFT was slowly injected intravenously over a period of 1 minute, before which a 2D-dynamic PET scan lasting for 60 minutes was commenced, with scan data obtained by 39 time frames (18 frames of 10 s, 6 frames of 30 s, 7 frames of 120 s, and 8 frames of 300 s). PET scans were performed on a PET scanner (ECAT ACCEL, Siemens Healthcare) that provided 47 slices in an axial field of view of 162 mm with an intrinsic transaxial resolution of 6.2 mm in full width at half maximum (64). The PET emission data were corrected for attenuation using the transmission data, and images were reconstructed in a matrix of 128, 128, 47 (x, y, z) with a voxel size of 0.86, 0.86, 3.38 mm (x, y, z) using a filtered back projection algorithm with a 2-mm Gaussian filter.

DAT binding in the brain was quantified voxel by voxel as a BP_{ND} image based on a simplified reference tissue model (65). The cerebellum was considered as a reference region and was identified by manual delineation of its boundary on a T1-weighted image that was pre-realigned to the time-integrated PET image. We also generated a tracer delivery image (R1) to be used for the next step of co-registration between the PET and MRI images. Calculation of BP_{ND} and R1 was performed using an open-source program (PyBLD; http://www.mi.med.osaka-u.ac.jp/pybld/pybld.html).

Tests for tumorigenicity and general conditions of engrafted animals. To assess the safety of our engrafting procedure, we performed blood tests, including red blood cell counts, white cell counts, and blood chemical tests, in all test animals to evaluate general conditions. We also analyzed the blood for several tumor markers among those tested in the clinic (66), including CEA, TPA, SLX, NSE, and BFP.

We also performed ^{18}F-FDG PET to assess any tumorigenic changes in the grafted area using a previously described method (18). After induction of anesthesia, we injected 185 MBq of ^{18}F-FDG and scanned the head region for a period from 40 to 60 minutes after injection. ^{18}F-FDG scans were performed in a 3D mode after the transmission scan. The reconstructed ^{18}F-FDG radioactivity image (in Bq/ml) was scaled based on the injected dose of ^{18}F-FDG per body weight of animal (Bq/g) to calculate images of standardized uptake value (SUV). The region was considered to be abnormal when the SUV was greater than 2.5 (67).

MRI. MRI was performed to enable MRI-guided stereotaxic surgery and evaluation of graft size after transplantation and for the analysis of PET data, using a 3-Tesla MRI scanner (Signa LX VAH/I, GE Healthcare). We obtained 3D T1-weighted MRI images from each animal with an IR-FSPGR sequence with imaging parameters as follows: TR = 9.4 ms, TE = 2.1 ms, TI = 600 ms, matrix = 128 × 128, field of view = 99.8 mm, slice thickness = 0.7 mm, number of slices = 100.

Immunohistochemical analysis of engrafted striatum. Nine months after transplantation, animals were sacrificed by overdose of pentobarbital and perfused transcardially with 4% paraformaldehyde in 0.1 M PBS. Brain tissues were cut into 10-μm-thick frozen coronal sections at the level of the posterior striatum (from y = −7 to −9 mm) using a cryostat. Primary antibodies used for immunohistochemistry were as follows: NeuN (1:150; Millipore), TH (1:1,200; DAKO), DAT (1:1,000; Millipore), GIRK2 (1:1,000; Chemicon, Millipore), calbindin (1:50; Swant), and Ki-67 (1:400; Thermo Scientific). Secondary antibodies were anti-rabbit IgG conjugated to Alexa Fluor 488 (Invitrogen), anti-rat IgG conjugated to Alexa Fluor 488 (Invitrogen), or anti-rabbit and anti-rat IgG conjugated to Cy3 (Jackson ImmunoResearch Laboratory). For triple staining for DAT/GIRK2/calbindin, calbindin was visualized using a anti-mouse IgG antibody conjugated to Alexa Fluor 680 (Invitrogen). Costaining with DAPI was also performed to confirm nuclear staining. For quantitative analysis, we chose 3 coronal sections, approximately located at y = −5, −7, −9 mm, and randomly selected 79–124 fields of view with an area of 0.316 × 0.316 mm^2 within the dorsal posterior putamen, and counted the number of cells stained for NeuN, TH, or DAT. The counts were compared among sections of striatum that received engraftments (MSC-DP group), those of sham-operated striatum (sham group), and those from the contralateral side of the striatum (non-MPTP–treated group) of sham-operated animals (nonaffected group). For counting TH$^+$ terminal density, images captured under a ×20 objective lens were imported into ImageJ (http://rsbweb.nih.gov/ij/); thereby, color was decomposed into red, green, and blue and thresholded for red based on the automatic isodata algorithm. To estimate the number of TH$^+$ terminals, the numbers of red particles, with sizes of >4 and <2,000 pixels (corresponding to >4 μm^2 and <4 × 10^6 μm^2), were counted. The data were expressed as the number of cells or axonal terminals per area (mm^2).

Statistics. Values are expressed as mean ± SEM. For immunohistochemistry and behavioral tests, data were analyzed using ANOVA. Differences among means were further analyzed by post-hoc multiple comparisons. The threshold for statistical significance was $P < 0.05$. Statistical analysis was performed using PRISM software (GraphPad Software Inc.).

For ^{11}C-CFT PET images, BP_{ND} images were preprocessed for voxel-based statistics using a previously described method (62). Briefly, the PET images were co-registered with MRI images (obtained at the time closest to the PET scan) using a rigid body transformation and transformed to the standard brain space of cynomolgus macaque (31). The transformation matrix of MRI images to the standard space was determined by an affine transformation algorithm. Voxel-based statistics were performed using a nonparametric permutation test (68) with 1-way ANOVA with repeated measures of BP_{ND} in the engrafted group. Permutation was performed within data from each subject, respecting the repeated-measures structure of the data. We are interested in the statistical F contrast for the effect of time in which FWE-corrected P values of less than 0.05 were applied using a threshold-free cluster enhancement (69). The significant cluster thus obtained (see Figure 3C) was used as a ROI for subsequent analyses (Figure 3, D–F). We also obtained BP_{ND} values from the contralateral (nonaffected) dorsal putamen as a control for BP_{ND} values, by ROI flipping (left-right) of the above cluster. The control values for BP_{ND} were 0.56 ± 0.12 (95% confidential interval, 0.51–0.61) in the engrafted group and 0.63 ± 0.11 (95% confidential interval, 0.59–0.67) in the sham group. Image analysis was performed using FSL tools (http://www.fmrib.ox.ac.uk/fsl).

The 1-hit model of neurodegeneration with a constant risk (32) was fitted to the time course data using BP_{ND} values obtained from the ROI in the engrafted striatum or using the graft volume of naive MSCs obtained from Figure 1 in ref. 13. The actual equation for the model was $V_G = V_0 \times exp(-ln[2] \times t/T_{1/2}) + Vp$, where the V_G is the time course of graft BP_{ND} or volume; V_0 is the initial value for V_G; exp is the exponential function; t is the time after grafting; $T_{1/2}$ is a half-life period; and Vp is plateau. Nonlinear fitting was performed using PRISM software.

Study approval. The experimental protocol and design of the study were in line with the institutional guides for animal experiments and the NIH Guide for the Care and Use of Laboratory Animals (NIH Publication No. 80-23) and were approved by the institutional committee for animal care and experiments of Tohoku University, RIKEN, and the National Cerebral and Cardiovascular Center.

Acknowledgments

We thank Noboru Teramoto, Hajime Fukuda, Hiroshi Koshino, Kyoko Shioya, Keiko Tokuda, and Akihiro Kawasaki for their technical help and Tsuyoshi Tahara and Hideki Mochizuki for their helpful comments. This study was supported by the Program for Promotion of Fundamental Studies in Health Sciences of the National Institute of Biomedical Innovation (NIBIO, 05-06, 10-05).

Received for publication July 13, 2012, and accepted in revised form September 28, 2012.

Address correspondence to: Takuya Hayashi, Functional Probe Research Laboratory, Center for Molecular Imaging Science, RIKEN, 6-7-3 Minnatojima-minamimachi, Chuo-ku, Kobe, Hyogo 650-0047, Japan. Phone: 81.78.304.7121; Fax: 81.78.304.7123; E-mail: takuya.hayashi@riken.jp. Or to: Mari Dezawa, Department of Stem Cell Biology and Histology and Department of Anatomy and Anthropology, Tohoku University Graduate School of Medicine, 2-1 Seiryo-machi, Aoba-ku, Sendai, Miyagi 980-8575, Japan. Phone: 81.22.717.8025; Fax: 81.22.717.8030; E-mail: mdezawa@med.tohoku.ac.jp.

1. Gage FH. Cell therapy. *Nature*. 1998; 392(6679 suppl):18–24.
2. Brundin P, Barker RA, Parmar M. Neural grafting in Parkinson's disease Problems and possibilities. *Prog Brain Res*. 2010;184:265–294.
3. Winkler C, Kirik D, Björklund A. Cell transplantation in Parkinson's disease: how can we make it work? *Trends Neurosci*. 2005;28(2):86–92.
4. Chen X, et al. Human bone marrow stromal cell cultures conditioned by traumatic brain tissue extracts: growth factor production. *J Neurosci Res*. 2002;69(5):687–691.
5. Pittenger MF, et al. Multilineage potential of adult human mesenchymal stem cells. *Science*. 1999;284(5411):143–147.
6. Charbord P. Bone marrow mesenchymal stem cells: historical overview and concepts. *Hum Gene Ther*. 2010;21(9):1045–1056.
7. Li Y, et al. Intracerebral transplantation of bone marrow stromal cells in a 1-methyl-4-phenyl-1,2,3,6-tetrahydropyridine mouse model of Parkinson's disease. *Neurosci Lett*. 2001;316(2):67–70.
8. Park HJ, Lee PH, Bang OY, Lee G, Ahn YH. Mesenchymal stem cells therapy exerts neuroprotection in a progressive animal model of Parkinson's disease. *J Neurochem*. 2008;107(1):141–151.
9. Blandini F, et al. Transplantation of undifferentiated human mesenchymal stem cells protects against 6-hydroxydopamine neurotoxicity in the rat. *Cell Transplant*. 2010;19(2):203–217.
10. Venkataramana NK, et al. Open-labeled study of unilateral autologous bone-marrow-derived mesenchymal stem cell transplantation in Parkinson's disease. *Transl Res*. 2010;155(2):62–70.
11. Kuroda Y, Kitada M, Wakao S, Dezawa M. Bone marrow mesenchymal cells: how do they contribute to tissue repair and are they really stem cells? *Arch Immunol Ther Exp (Warsz)*. 2011;59(5):369–378.
12. Wagner W, et al. Replicative senescence of mesenchymal stem cells: a continuous and organized process. *PLoS One*. 2008;3(5):e2213.
13. Moloney TC, et al. Survival and immunogenicity of mesenchymal stem cells from the green fluorescent protein transgenic rat in the adult rat brain. *Neurorehabil Neural Repair*. 2010;24(7):645–656.
14. Thompson L, Barraud P, Andersson E, Kirik D, Björklund A. Identification of dopaminergic neurons of nigral and ventral tegmental area subtypes in grafts of fetal ventral mesencephalon based on cell morphology, protein expression, and efferent projections. *J Neurosci*. 2005;25(27):6467–6477.
15. Mendez I, et al. Cell type analysis of functional fetal dopamine cell suspension transplants in the striatum and substantia nigra of patients with Parkinson's disease. *Brain*. 2005;128(pt 7):1498–1510.
16. Grealish S, et al. The A9 dopamine neuron component in grafts of ventral mesencephalon is an important determinant for recovery of motor function in a rat model of Parkinson's disease. *Brain*. 2010; 133(pt 2):482–495.
17. Damier P, Hirsch EC, Agid Y, Graybiel AM. The substantia nigra of the human brain. II. Patterns of loss of dopamine-containing neurons in Parkinson's disease. *Brain*. 1999;122(pt 8):1437–1448.
18. Wakao S, et al. Long-term observation of auto-cell transplantation in non-human primate reveals safety and efficiency of bone marrow stromal cell-derived Schwann cells in peripheral nerve regeneration. *Exp Neurol*. 2010;223(2):537–547.
19. Hayase M, et al. Committed neural progenitor cells derived from genetically modified bone marrow stromal cells ameliorate deficits in a rat model of stroke. *J Cereb Blood Flow Metab*. 2009; 29(8):1409–1420.
20. Dezawa M, et al. Specific induction of neuronal cells from bone marrow stromal cells and application for autologous transplantation. *J Clin Invest*. 2004; 113(12):1701–1710.
21. Nagane K, Kitada M, Wakao S, Dezawa M, Tabata Y. Practical induction system for dopamine-producing cells from bone marrow stromal cells using spermine-pullulan-mediated reverse transfection method. *Tissue Eng Part A*. 2009;15(7):1655–1665.
22. Sladek JR Jr, Collier TJ, Haber SN, Roth RH, Redmond DE Jr. Survival and growth of fetal catecholamine neurons transplanted into primate brain. *Brain Res Bull*. 1986;17(6):809–818.
23. Redmond DE, et al. Fetal neuronal grafts in monkeys given methylphenyltetrahydropyridine. *Lancet*. 1986;1(8490):1125–1127.
24. Bankiewicz KS, et al. The effect of fetal mesencephalon implants on primate MPTP-induced parkinsonism. Histochemical and behavioral studies. *J Neurosurg*. 1990;72(2):231–244.
25. Kordower JH, et al. Neurodegeneration prevented by lentiviral vector delivery of GDNF in primate models of Parkinson's disease. *Science*. 2000; 290(5492):767–773.
26. Takagi Y, et al. Dopaminergic neurons generated from monkey embryonic stem cells function in a Parkinson primate model. *J Clin Invest*. 2005; 115(1):102–109.
27. Eberling JL, et al. Functional effects of AAV2-GDNF on the dopaminergic nigrostriatal pathway in parkinsonian rhesus monkeys. *Hum Gene Ther*. 2009; 20(5):511–518.
28. Ferri ALM, et al. Foxa1 and Foxa2 regulate multiple phases of midbrain dopaminergic neuron development in a dosage-dependent manner. *Development*. 2007;134(15):2761–2769.
29. McRitchie DA, Hardman CD, Halliday GM. Cytoarchitectural distribution of calcium binding proteins in midbrain dopaminergic regions of rats and humans. *J Comp Neurol*. 1996;364(1):121–150.
30. Bankiewicz KS, et al. Hemiparkinsonism in monkeys after unilateral internal carotid artery infusion of 1-methyl-4-phenyl-1,2,3,6-tetrahydropyridine (MPTP). *Life Sci*. 1986;39(1):7–16.
31. Frey S, et al. An MRI based average macaque monkey stereotaxic atlas and space (MNI monkey space). *Neuroimage*. 2011;55(4):1435–1442.
32. Clarke G, et al. A one-hit model of cell death in inherited neuronal degenerations. *Nature*. 2000; 406(6792):195–9.
33. Burbach JPH, Smidt MP. Molecular programming of stem cells into mesodiencephalic dopaminergic neurons. *Trends Neurosci*. 2006;29(11):601–603.
34. Lindvall O, et al. Grafts of fetal dopamine neurons survive and improve motor function in Parkinson's disease. *Science*. 1990;247(4942):574–577.
35. Freed CR, et al. Survival of implanted fetal dopamine cells and neurologic improvement 12 to 46 months after transplantation for Parkinson's disease. *N Engl J Med*. 1992;327(22):1549–1555.
36. Peschanski M, et al. Bilateral motor improvement and alteration of L-dopa effect in two patients with Parkinson's disease following intrastriatal transplantation of foetal ventral mesencephalon. *Brain*. 1994;117(pt 3):487–499.
37. Spencer DD, et al. Unilateral transplantation of human fetal mesencephalic tissue into the caudate nucleus of patients with Parkinson's disease. *N Engl J Med*. 1992;327(22):1541–1548.
38. Freed CR, et al. Transplantation of embryonic dopamine neurons for severe Parkinson's disease. *N Engl J Med*. 2001;344(10):710–719.
39. Olanow CW, et al. A double-blind controlled trial of bilateral fetal nigral transplantation in Parkinson's disease. *Ann Neurol*. 2003;54(3):403–414.
40. Li J-Y, Christophersen NS, Hall V, Soulet D, Brundin P. Critical issues of clinical human embryonic stem cell therapy for brain repair. *Trends in Neurosciences*. 2008;31(3):146–153.
41. Vinuela A, et al. Implanted reuptake-deficient or wild-type dopaminergic neurons improve ON L-dopa dyskinesias without OFF-dyskinesias in a rat model of Parkinson's disease. *Brain*. 2008; 131(pt 12):3361–3379.
42. Kittappa R, Chang WW, Awatramani RB, McKay RDG. The foxa2 gene controls the birth and spontaneous degeneration of dopamine neurons in old age. *PLoS Biol*. 2007;5(12):e325.
43. Cooper O, et al. Differentiation of human ES and Parkinson's disease iPS cells into ventral midbrain dopaminergic neurons requires a high activity form of SHH, FGF8a and specific regionalization by retinoic acid. *Mol Cell Neurosci*. 2010;45(3):258–266.
44. Cai J, et al. The role of Lmx1a in the differentiation of human embryonic stem cells into midbrain dopamine neurons in culture and after transplantation into a Parkinson's disease model. *Stem Cells*. 2009;27(1):220–229.
45. Hargus G, et al. Differentiated Parkinson patient-derived induced pluripotent stem cells grow in the adult rodent brain and reduce motor asymmetry in Parkinsonian rats. *Proc Natl Acad Sci USA*. 2010; 107(36):15921–15926.
46. Sonntag K-C, et al. Context-dependent neuronal differentiation and germ layer induction of Smad4$^{-/-}$ and Cripto$^{-/-}$ embryonic stem cells. *Mol Cell Neurosci*. 2005;28(3):417–429.
47. Kriks S, et al. Dopamine neurons derived from human ES cells efficiently engraft in animal models of Parkinson's disease. *Nature*. 2011;480(7378):547–551.
48. O'Keeffe FE, et al. Induction of A9 dopaminergic neurons from neural stem cells improves motor function in an animal model of Parkinson's disease. *Brain*. 2008;131(pt 3):630–641.
49. Kuan W-L, Lin R, Tyers P, Barker RA. The importance of A9 dopaminergic neurons in mediating the functional benefits of fetal ventral mesencephalon transplants and levodopa-induced dyskinesias. *Neurobiol Dis*. 2007;25(3):594–608.
50. De Camilli P, Miller PE, Navone F, Theurkauf WE, Vallee RB. Distribution of microtubule-associated protein 2 in the nervous system of the rat studied by immunofluorescence. *Neuroscience*. 1984; 11(4):817–846.
51. Xu H, et al. Transplantation of neuronal cells induced from human mesenchymal stem cells improves neurological functions after stroke without cell fusion. *J Neurosci Res*. 2010;88(16):3598–3609.
52. Freeman TB, Brundin P. Important aspects of surgical methodology for transplantation in Parkinson's disease. In: Brundin P, Olanow CW, eds. *Restorative Therapies in Parkinson's Disease*. New York, New York, USA: Springer; 2006:131–165.
53. Dubach M, et al. Primate neostriatal neurons containing tyrosine hydroxylase: immunohistochemical evidence. *Neurosci Lett*. 1987;75(2):205–210.
54. Guliás B, Halldin C. New PET radiopharmaceuticals beyond FDG for brain tumor imaging. *Q J Nucl Med Mol Imaging*. 2012;56(2):173–190.
55. Padma MV, et al. Functional imaging of a large demyelinating lesion. *J Clin Neurosci*. 2005;12(2):176–178.
56. Lewis DA, Sesack SR. Dopamine systems in the primate brain. In: Bloom FE, Björklund A, Hökfelt T. *The Primate Nervous System*. New York, New York, USA: Elsevier; 1997:263–375.
57. Kordower JH, Liu YT, Winn S, Emerich DF. Encapsulated PC12 cell transplants into hemiparkinsonian monkeys: a behavioral, neuroanatomical, and neurochemical analysis. *Cell Transplant*. 1995; 4(2):155–171.
58. Luthman J, Jonsson G. Effects of the parkinsonism-inducing neurotoxin MPTP and its metabolite MPP+ on sympathetic adrenergic nerves in mouse iris and atrium. *Med Biol*. 1986;64(2–3):95–102.
59. Kurlan R, Kim MH, Gash DM. Oral levodopa dose-response study in MPTP-induced hemiparkinsonian monkeys: assessment with a new rating scale for monkey parkinsonism. *Mov Disord*. 1991;6(2):111–118.
60. Jordan S, et al. 6-[18F]fluoro-L-m-tyrosine: metab-

olism, positron emission tomography kinetics, and 1-methyl-4-phenyl-1,2,3,6-tetrahydropyridine lesions in primates. *Brain Res.* 1997;750(1–2):264–276.
61. Emborg ME, et al. Age-related declines in nigral neuronal function correlate with motor impairments in rhesus monkeys. *J Comp Neurol.* 1998; 401(2):253–265.
62. Saiki H, Hayashi T, Takahashi R, Takahashi J. Objective and quantitative evaluation of motor function in a monkey model of Parkinson's disease. *J Neurosci Methods.* 2010;190(2):198–204.
63. Någren K, Müller L, Halldin C, Swahn CG, Lehikoinen P. Improved synthesis of some commonly used PET radioligands by the use of [11C] methyl triflate. *Nucl Med Biol.* 1995;22(2):235–239.
64. Herzog H, et al. NEMA NU2-2001 guided performance evaluation of four Siemens ECAT PET scanners. *IEEE Trans Nucl Sci.* 2004;51(5):2662–2669.
65. Gunn RN, Lammertsma AA, Hume SP, Cunningham VJ. Parametric imaging of ligand-receptor binding in PET using a simplified reference region model. *Neuroimage.* 1997;6(4):279–287.
66. Sturgeon C. Practice guidelines for tumor marker use in the clinic. *Clin Chem.* 2002;48(8):1151–1159.
67. Al-Sugair A, Coleman RE. Applications of PET in lung cancer. *Semin Nucl Med.* 1998;28(4):303–319.
68. Nichols TE, Holmes AP. Nonparametric permutation tests for functional neuroimaging: a primer with examples. *Hum Brain Mapp.* 2002;15(1):1–25.
69. Smith SM, Nichols TE. Threshold-free cluster enhancement: addressing problems of smoothing, threshold dependence and localisation in cluster inference. *Neuroimage.* 2009;44(1):83–98.

OPEN ACCESS Freely available online

PLOS | ONE

Morphologic and Gene Expression Criteria for Identifying Human Induced Pluripotent Stem Cells

Shohei Wakao[1]*, Masaaki Kitada[1], Yasumasa Kuroda[2], Fumitaka Ogura[1], Toru Murakami[1], Akira Niwa[3], Mari Dezawa[1,2]*

1 Department of Stem Cell Biology and Histology, Tohoku University Graduate School of Medicine, Sendai, Miyagi, Japan, **2** Department of Anatomy and Anthropology, Tohoku University Graduate School of Medicine, Sendai, Miyagi, Japan, **3** Center for iPS Cell Research and Application, Kyoto University, Kyoto, Japan

Abstract

Induced pluripotent stem (iPS) cells can be generated from somatic cells by the forced expression of four factors, Oct3/4, Sox2, Klf4, and c-Myc. While a great variety of colonies grow during induction, only a few of them develop into iPS cells. Researchers currently use visual observation to identify iPS cells and select colonies resembling embryonic stem (ES) cells, and there are no established objective criteria. Therefore, we exhaustively analyzed the morphology and gene expression of all the colonies generated from human fibroblasts after transfection with four retroviral vectors encoding individual factors (192 and 203 colonies in two experiments) and with a single polycistronic retroviral vector encoding all four factors (199 and 192 colonies in two experiments). Here we demonstrate that the morphologic features of emerged colonies can be categorized based on six parameters, and all generated colonies that could be passaged were classified into seven subtypes in colonies transfected with four retroviral vectors and six subtypes with a single polycistronic retroviral vector, both including iPS cell colonies. The essential qualifications for iPS cells were: cells with a single nucleolus; nucleus to nucleolus (N/Nls) ratio ~2.19: cell size ~43.5 μm^2: a nucleus to cytoplasm (N/C) ratio ~0.87: cell density in a colony ~5900 cells/mm^2: and number of cell layer single. Most importantly, gene expression analysis revealed for the first time that endogenous Sox2 and Cdx2 were expressed specifically in iPS cells, whereas Oct3/4 and Nanog, popularly used markers for identifying iPS cells, are expressed in colonies other than iPS cells, suggesting that Sox2 and Cdx2 are reliable markers for identifying iPS cells. Our findings indicate that morphologic parameters and the expression of endogenous Sox2 and Cdx2 can be used to accurately identify iPS cells.

Citation: Wakao S, Kitada M, Kuroda Y, Ogura F, Murakami T, et al. (2012) Morphologic and Gene Expression Criteria for Identifying Human Induced Pluripotent Stem Cells. PLoS ONE 7(12): e48677. doi:10.1371/journal.pone.0048677

Editor: Martin Pera, University of Melbourne, Australia

Received June 19, 2012; **Accepted** September 28, 2012; **Published** December 13, 2012

Funding: This study was supported by a Grant-in-Aid for Scientific Research (23390060) from the Ministry of Education, Culture Sports, Science, and Technology, Japan. The funders had no role in study design, data collection and analysis, decision to publish, or preparation of the manuscript.

Competing Interests: The authors have declared that no competing interests exist.

* E-mail: wakao@med.tohoku.ac.jp (SW); mdezawa@med.tohoku.ac.jp (MD)

Introduction

Embryonic stem (ES) cells derived from the inner cell mass of blastocysts are able to self-renew and differentiate into cells representative of all three germ layers, indicating that they are pluripotent stem cells [1,2]. While they are expected to contribute to cell-based therapy due to their ability to differentiate into a great variety of cells, ethical considerations relating to the use of fertilized eggs pose limitations for their practical use. Induced pluripotent stem (iPS) cells can be generated from adult human somatic cells by introducing factors such as Oct3/4, Sox2, Klf-4, and c-Myc (the four so-called Yamanaka factors), and like ES cells, iPS cells are able to self-renew and differentiate into cells representative of all three germ layers [3]. iPS cells have many advantages and the ethical concerns regarding the use of fertilized eggs are eliminated. Disease-specific iPS cells generated from patients are also expected to be applicable for the evaluation of disease mechanisms and drug efficacy [4,5].

Introduction of the four Yamanaka factors to cells cultured on feeder cells induces the development of colonies of cells with a variety of morphologies, but only a few of them have ES cell-like morphology and are thus identified as iPS cells. Usually, only those colonies with ES cell-like morphologies are picked up and further cultured for the generation of iPS cells, while colonies with a non-ES cell-like morphology are ignored because they are not considered to contribute to iPS cell generation and have thus not been analyzed in detail. Although these cells do not directly contribute to iPS cell generation, some intracellular changes might be caused by the introduction of the four Yamanaka factors, so that investigating the similarities and differences between these colonies and iPS cell colonies will be advantageous toward understanding iPS cells.

Analysis of the genes expressed by all colonies appearing during the generation of iPS cells was reported previously [6], but studies evaluating the morphologic characteristics in addition to the gene expression pattern of all the generated colonies have not been reported. Furthermore, ES cell-like colonies are most often judged under microscopic observation, and there are no objective criteria or parameters for identifying iPS cells. With regard to gene expression, the basis for iPS cell generation efficiency differs among reports; some reports calculate generation efficiency based only on alkaline phosphatase staining, whereas others are based on the expression of a reporter gene driven by the promoter of a single pluripotency marker such as Nanog or Oct3/4 [7,8,9]. Therefore, the reported generation efficiencies cannot be com-

pared with each other and reliable markers or parameters for iPS cells must be defined.

In the present study, we transduced the four Yamanaka factors to adult human skin-derived fibroblasts using either four retroviral vectors encoding Oct3/4, Sox2, Klf4, and c-Myc, or a single polycistronic Oct3/4-Klf4-Sox2-c-Myc-GFP expressing viral vector, and subjected the fibroblasts to iPS cell generation procedures. After gene transduction, all generated colonies, including ES cell-like colonies, namely iPS cell colonies, were classified based on six morphologic parameters. We further performed gene expression analyses of each categorized colony and explored the elements available for identifying iPS cells. We show that the morphologic features specific for iPS cell colonies are objectively represented. Moreover, the expression of either Oct3/4 or Nanog, which are currently often used to identify iPS cells, is not appropriate for the identification of iPS cells, but rather the expression of endogenous Sox2 and Cdx2 is a reliable marker of iPS cells. Our results indicate that combined evaluation of morphologic parameters and gene expression of endogenous Sox2 and Cdx2 is useful for accurately identifying iPS cells and will greatly contribute to a better understanding of iPS cells.

Results

Yamanaka four factors Oct3/4, Sox2, Klf4, and c-Myc were transduced to adult human dermal fibroblasts with four retroviral vectors or with a single polycistronic retroviral vector according to the original method [3,10]. Five days after transduction, cells were transferred onto inactivated mouse embryonic fibroblasts and cultured in ES cell medium. Thirty days after the transduction with four retroviral vectors, 202 and 215 colonies were generated in two experiments respectively and each colony was picked up for further culturing. Ten and twelve colonies failed to be passaged, respectively, and the remaining 192 and 203 colonies were subjected to further analysis after two passages. In the case of the single polycistronic vector transduction, 199 and 192 colonies were obtained in two experiments respectively and all colonies were picked, passaged twice and analyzed.

We considered the morphologic characteristics that indicate ES cell-like cells and colonies, and set 6 parameters: 1) number of nucleoli, 2) nucleus to nucleolus (N/Nls) ratio 3) cell size, 4) cell density (cells/mm^2), 5) nucleus to cytoplasm (N/C) ratio and 6) number of cell layers (multilayer or monolayer) of the colony, all of which are considered necessary elements for distinguishing ES cell-like colonies from among various other types of colonies. Following these parameters, we performed a morphometric analysis of randomly selected five cells from the central region of each colony.

Human ES cell colonies were firstly analyzed as a control, and resulted as follows: number of nucleoli 1.20±0.45; N/Nls ratio 2.20±0.17; cell size 43.70±3.61 μm^2; cell density 6133.33±15.32 cells/mm^2; N/C ratio 0.86±0.04; and single cell layer (Table 1).

We classified an ES cell-like colony, namely an iPS cell colony, as colony G for both four retroviral vectors (2 colonies) and a single polycistronic vector (2 colonies). The mean parameter values of four colonies in colony G were: number of nucleoli 1.20±0.45; N/Nls ratio 2.19±0.17; cell size 43.50±2.96 μm^2; cell density 5933.33±20.82 cells/mm^2; N/C ratio 0.87±0.04; and single cell layer; indicating that each parameter in colony G was statistically identical to those of human ES cells ($p<0.05$ with Bonferroni's correction; Table 1). Cells in colony G expressed the pluripotency markers Oct3/4, Nanog, Sox2, and TRA-1-81 in immunocytochemistry (Fig. 1A–D), differentiated *in vitro* into cells representa-

Table 1. Classification of morphologic characteristics of colonies generated from human fibroblasts using four retroviral vectors encoding Oct3/4, Sox2, Klf4, and c-Myc.

	number of nucleolus	nucleus to nucleolus ratio	cell size	cell density/mm^2	nucleus to cytoplasm ratio	number of layer	number of colonies obtained (Experiment 1)	number of colonies obtained (Experiment 2)
Col A	2.35±0.51	3.30±0.48	87.69±11.04	2166.67±29.21	0.59±0.07	multilayer	16	22
Col B	1.46±0.59	2.95±0.41	113.20±13.40	1863.06±22.49	0.53±0.06	multilayer	55	49
Col C	1.34±0.55	2.50±0.50	69.82±9.29	3048.96±26.14	0.60±0.07	multilayer	95	102
Col D	1.33±0.47	3.17±0.50	52.09±7.69	5091.67±21.65	0.6±0.05	multilayer	6	8
Col E	1.24±0.48	2.52±0.43	45.72±7.14	3493.33±24.03	0.59±0.07	multilayer	10	8
Col F	1.27±0.49	2.42±0.23	58.34±5.92	5266.67±41.01	0.64±0.06	multilayer	8	12
Col G (iPS cell)	1.20±0.45	2.19±0.17	43.50±2.96	5933.33±20.82	0.87±0.04	single	2	2
human ES cell	1.20±0.45	2.20±0.17	43.70±3.61	6133.33±15.32	0.86±0.04	single		

Each replicate represented 2×10^5 transduced cells seeded onto a 60-mm dish containing feeder cells and cultured in Primate ES cell medium for thirty days.

doi:10.1371/journal.pone.0048677.t001

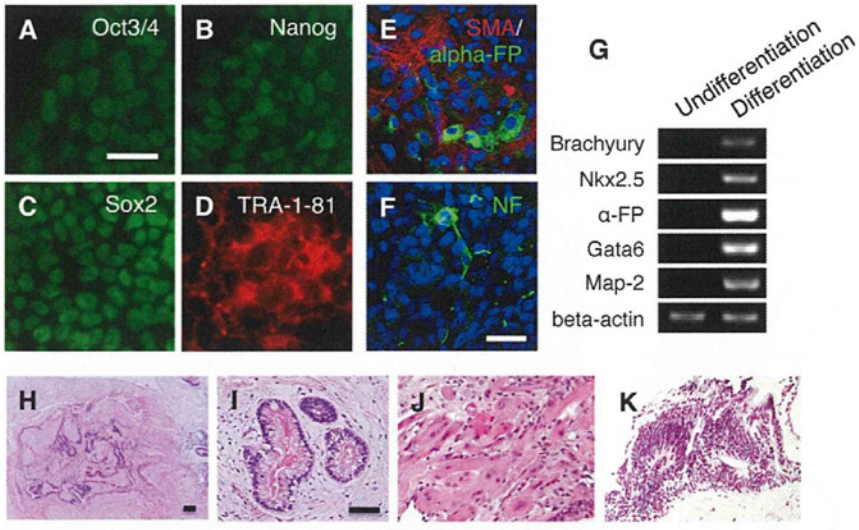

Figure 1. Characterization of iPS cell colony G. (A–D) Immunocytochemistry for (A) Oct3/4, (B) Nanog, (C) Sox2, (D) TRA-1-81 in iPS cell colony G. Scale bar = 100 μm. (E, F) EBs generated from colony G were plated on gelatin coated dishes containing DMEM/F12 medium supplemented with 20% knockout serum replacement. After 10 days, cell differentiation was confirmed by immunocytochemistry for mesodermal (smooth muscle actin; SMA) (E), endodermal (alpha-fetoprotein; alpha-FP) (E) and ectodermal markers (neurofilament; NF) (F). Scale bar = 100 μm. (G) RT-PCR of differentiation markers in undifferentiated iPS cell colony G (Undifferentiation) and embryoid bodies derived from iPS cell colony G. Differentiation). (H–K) Hematoxylin and eosin staining of teratoma formed by transplantation of iPS cell colony G into immunodeficient mice testis. (H), Low magnification of the formed teratoma (12 weeks after injection). Endodermal (I), mesodermal (J) and ectodermal (K) tissue were observed in the teratoma.
doi:10.1371/journal.pone.0048677.g001

tive of all three germ layers (Fig. 1E–G), and formed teratomas when transplanted into immunodeficient mouse testis (Fig. 1H–K).

Besides two colonies that were already determined as colony G, remaining 190 and 201 colonies generated by four retroviral vectors were analyzed. The average and standard deviation of number of nucleolus, N/Nls ratio, cell size, cell density and N/C ratio in each colony were compared to those of colony G by t-test and all the colonies were sorted according to the number and content of parameters that showed significant statistical differences. As a result, colonies were categorized into 6 typical types, colony A~F. When iPS cell colony G and the rest of the colonies A~F were compared, iPS cells showed maximum value in cell density and N/C ratio, whereas cell size, number of nucleoli and N/Nls ratio were minimum. In addition to above 5 parameters, number of cell layer was also analyzed. In contrast to iPS cell colony G and ES cells that demonstrated single cell layer, colony A~F piled up to form multiple layers. The parameters for each type of colony are shown in Table 1. The characteristics of each colony in terms of significant statistical differences to colony G are summarized as follows: colony A, number of nucleoli, N/Nls ratio, cell size, cell density, N/C ratio showed significant difference to those of colony G ($p<0.01$); colony B, N/Nls ratio, cell size, cell density, N/C ratio ($p<0.01$); colony C, cell size, cell density, N/C ratio ($p<0.01$); colony D, N/Nls ratio, cell density, N/C ratio ($p<0.01$); colony E, cell density, N/C ratio ($p<0.01$); colony F, cell size, N/C ratio ($p<0.01$) (Fig. 2A–G).

Gene expression of pluripotency markers was evaluated in colonies A~G using reverse transcription-polymerase chain reaction (RT-PCR). We analyzed 10 genes that are reportedly expressed in both human ES and iPS cells [10,11,12,13,14]: endogenous Oct3/4, endogenous Sox2, Nanog, endogenous Klf4, endogenous c-Myc, FoxD3 (Forkhead box D3), Rex1 (Zfp42), Dnmt3b (DNA (cytosine-5-)-methyltransferase 3 beta), Abcg2 (ATP-binding cassette sub-family G member 2), and Cdx2 (caudal-type homeobox protein 2).

Adult human dermal fibroblasts endogenously expressed Klf4 and c-Myc but not any other genes (data not shown). Colonies A~F and iPS cell colony G also expressed Klf4 and c-Myc, indicating that these two genes were expressed from the beginning of the human dermal fibroblasts and their expression was maintained even after receiving the four Yamanaka factors, regardless of the colony type (Fig. 3A). Genes such as endogenous Oct3/4, endogenous Sox2, and Nanog, which cooperatively maintain self-renewal and pluripotent states in pluripotent stem cells, are known to be downregulated upon their differentiation [15,16,17]. In colonies A~F, lower expression of endogenous Oct3/4 compared to iPS cell colony G was seen (Fig. 3A). It is noteworthy that, in colony B, Nanog expression was detected whereas endogenous Sox2 was not. Only iPS cell colony G expressed three sets of genes, namely endogenous Oct3/4, endogenous Sox2, and Nanog, and colonies A~F consistently did not express Sox2 (Fig. 3A). As for FoxD3, Rex1, Dnmt3b, Abcg2, and Cdx2, none of the colonies A~F expressed all 5 of these genes and in most cases, some were positive but others were negative. Importantly, like with Sox2, none of these colonies expressed Cdx2. Only iPS cell colony G expressed all the genes, including Sox2 and Cdx2 (Fig. 3A). These results were confirmed by quantitative-PCR (Q-PCR). In each fold expression calculation, the cyclethreshold (Ct) value of each genes expression in all colonies and human ES cells were compared to the average Ct value of each genes expression in adult human dermal fibroblasts (Fib.3B). Cdx2 is known to be required for differentiation of trophectoderm, and is reported not to be detected in undifferentiated human ES cells [18]. Consistent with this previous report, our result showed that the expression of Cdx2 was not detectable in undifferentiated human ES cells (Fig. 3B). On the other hand, the expression of endogenous Cdx2 was consistently detectable

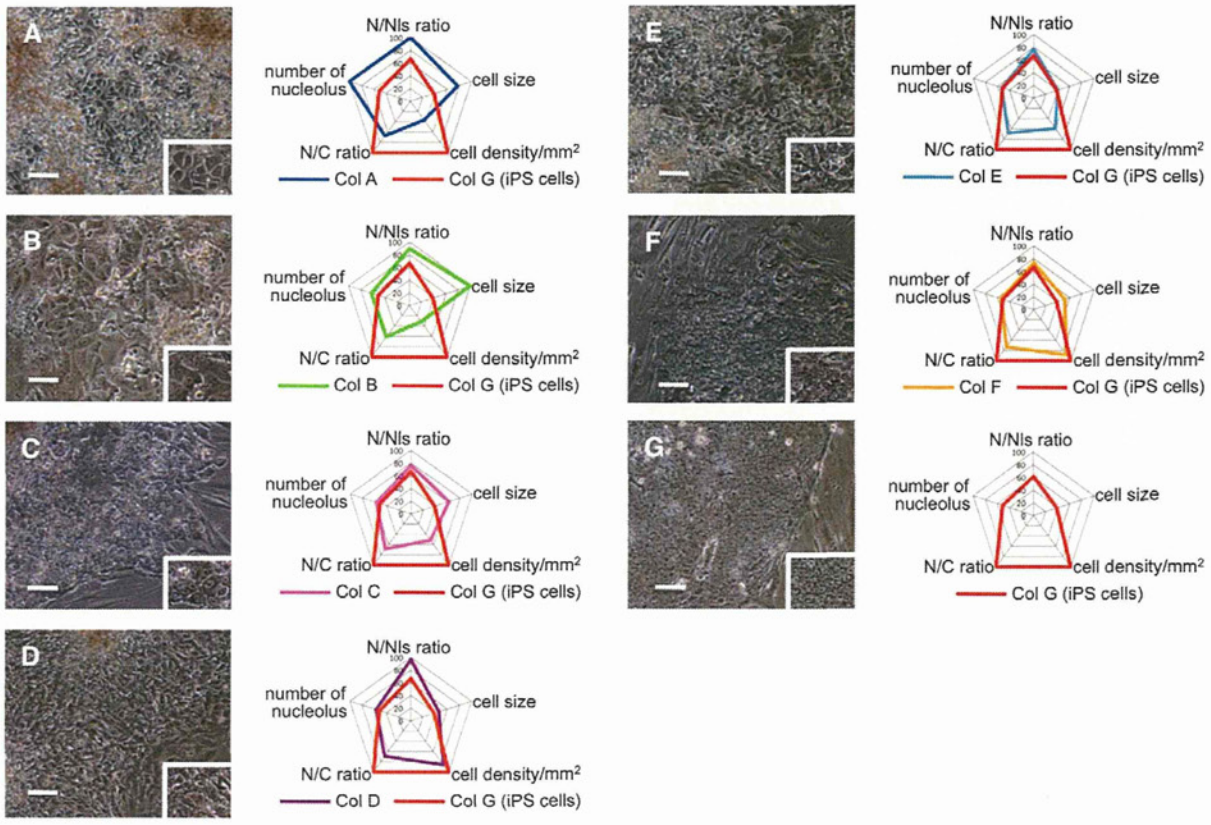

Figure 2. Morphometric analysis of colonies generated from human fibroblasts using four retroviral vectors encoding Oct3/4, Sox2, Klf4, and c-Myc. (A–G) Photographs and parameters of colonies A~G. Graphs shows parameters of each classified colony, including that of iPS cell colony G. The numerical value in the graph indicate the ratio to the maximum value (setting 100 for maximum value) in each parameters. N/Nls = nucleus-to-nucleolus ratio; N/C = nucleus-to-cytoplasm ratio. Scale bars = 100 μm.
doi:10.1371/journal.pone.0048677.g002

only in iPS cell colony G (Fig. 3B). Overall, the data obtained in Q-PCR showed same tendency to those in RT-PCR (Fig. 3B).

The formation of embryoid bodies (EBs) *in vitro* is a very important step for pluripotent stem cells to elicit their differentiation. EBs are usually formed in human pluripotent stem cells by culturing a single colony-derived small fragment containing 50 to 200 cells in suspension (Harvard Stem Cell Institute iPS Cell Core Facility; http://www.hsci.harvard.edu/ipscore/node/8). After culturing in suspension for 10 days, human pluripotent stem cells gradually expand and form EBs of at least 300 μm in diameter [19]. We tried to form EBs from colonies A~G to verify their ability to differentiate. Large cell clusters with diameters greater than 300 μm were formed in iPS colony G (Fig. S1A), while cell clusters whose sizes were less than 90 μm were formed by single colony-derived small fragments in colonies A~F, and these cell clusters did not continue to grow in suspension culture (Fig. S1B). When the formed cell clusters were transferred to gelatin-coated dishes, EBs from iPS cell colony G adhered to the bottom of the dish and the cells differentiated into endodermal (alpha-fetoprotein, GATA6), ectodermal (neurofilament, MAP-2), and mesodermal cells (smooth muscle actin, Brachyury, Nkx2.5) (Fig. 1E, F, G). On the other hand, all the cell clusters formed from colonies A~F dispersed or degenerated so that adhesion of these cell clusters to the dish and their triploblastic differentiation were never confirmed. Based on these results, we concluded that the cell clusters that formed from iPS cell colony G were EBs because they expanded and differentiated into cells representative of all three germ layers, while cell clusters formed from colonies A~F did not appear to form EBs, because they showed no further growth in suspension. Therefore, colonies A~F were not considered to be iPS cells.

Because the transduction of all four individual Oct3/4, Sox2, Klf-4, and c-Myc retroviruses into the cells by the four retroviral vectors might not be successful, we repeated the analysis by transducing a single polycistronic viral vector encoding Oct3/4-Klf4-Sox2-c-Myc-GFP into the cells [10]. Transduced cells were isolated by fluorescence-activated cell sorting based on green fluorescent protein gene expression, and then subjected to the iPS cell generation procedure. Cells in 199 and 192 colonies were morphometrically analyzed based on the above six parameters. The morphometric data obtained from all of these colonies, except for the colonies categorized as colony G, were statitstically different from those of the colonies generated by four retroviral vectors encoding Oct3/4, Sox2, Klf4, and c-Myc individually, namely colonies A~F. and therefore, we newly categorized them into five subtypes, that is, colonies H~L. Colony H showed statistically significant difference to colony G in N/Nls ratio, cell size, cell density and N/C ratio ($p<0.01$). In colony I, cell size, cell density, N/C ratio ($p<0.01$), in colony J, cell density and N/C ratio ($p<0.01$), colony K, cell size and N/C ratio ($p<0.01$), and colony L, only N/C ratio ($p<0.01$) (Table 2, Fig. 4H–L). As for the

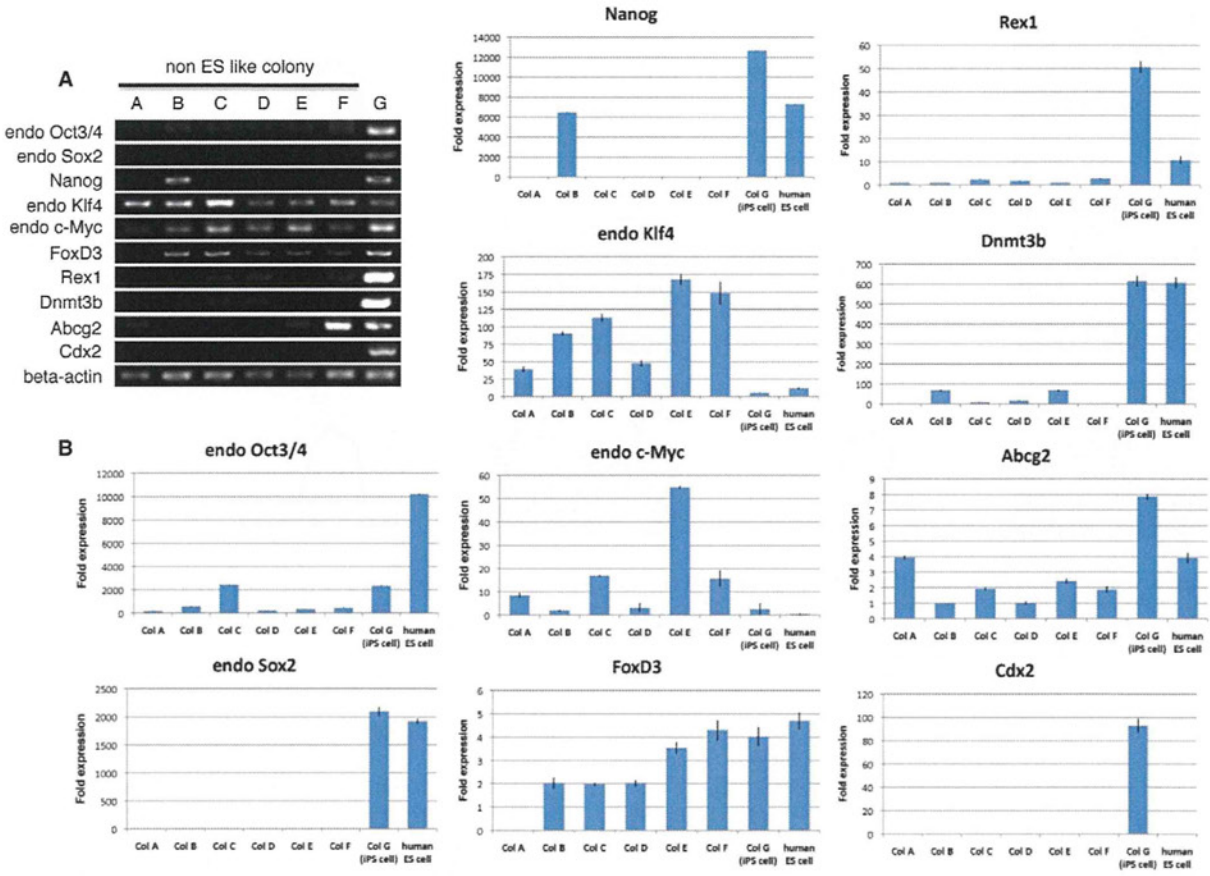

Figure 3. RT-PCR and Q-PCR of typical examples in each of colonies A~F, iPS cell colony G and human ES cells. (A) RT-PCR analysis examined the expression of endogenous Oct3/4, Sox2, Nanog, Klf4, c-Myc, as well as FoxD3, Rex1, Dnmt3b, Abcg2 and Cdx2. Beta-actin was used as an internal control. (B) Q-PCR data for expression of endogenous Oct3/4, Sox2, Nanog, Klf4, c-Myc, as well as FoxD3, Rex1, Dnmt3b, Abcg2 and Cdx2. Beta-actin was used as an internal control.
doi:10.1371/journal.pone.0048677.g003

number of cell layers, colonies H, I and K had a monolayer while colonies J and L had multiple cell layers (Table. 2).

RT-PCR demonstrated that colonies H, I, K, and L expressed endogenous Oct3/4 with weaker intensity than that in iPS cell colony G, and that colonies H, I, J, and L expressed Nanog while none of colonies H~L expressed endogenous Sox2 (Fig. 5A). These findings were further confirmed by Q-PCR. The expression of endogenous Oct3/4 was detected in all colonies. The expression level of endogenous Oct3/4 was three to ten times lower than that in iPS cell colony G, and that of Nanog in colonies H, I and L ranged from being almost equivalent to up to two to five times higher than that in iPS cell colony G (Fig. 5B). However, the expression of Sox2 was consistently undetectable in colonies H~L (Fig. 5B).

Colony J expressed FoxD3, Rex1, Dnmt3b, and Abcg2, while colonies H, I, K and L expressed some combination of two or three of these genes (Fig. 5A). Importantly, like Sox2, Cdx2 expression could not be detected in colonies H~L, while only iPS cell colony G expressed Cdx2 (Fig. 5A,B). Furthermore, we performed suspension culture in colonies H~L. As described above, single colony-derived small fragments from colonies H~L did not show further growth to form EB-like cell clusters in suspension culture (data not shown).

Discussion

The polycistronic vector reduced the variation in morphologic categorization but induced different morphologic features and gene expression patterns compared with those obtained with individual Oct3/4, Sox2, Klf-4, and c-Myc retroviruses. In our case, all the colonies arising during iPS cell generation could be categorized morphologically into 1 of 12 colony types. Common among colonies A~L, the non-ES cell-like colonies did not express endogenous Sox2 and Cdx2, while in contrast, iPS cell colony G consistently expressed both genes.

We conclude that the criteria to determine iPS cell colonies can be summarized as follows: number of nucleoli 1.20 ± 0.45; N/Nls ratio 2.19 ± 0.17; cell size $43.50\pm2.96\ \mu m^2$; cell density 5933.33 ± 20.82 cells/mm^2; N/C ratio 0.87 ± 0.04; and single cell layer; and cells positive for endogenous Sox2 and Cdx2. For further confirmation, the expression of other pluripotency-related factors, endogenous Oct3/4, Nanog, FoxD3, Rex1, Dnmt3b, and Abcg2, will be useful.

Up to now, iPS cell colonies are visually identified as the flat cell colonies with defined edge and tightly packed cells [3]. Such identification would be dependent on ones subjective judgment and would not be reliable objective criteria. In this report, based on morphologically objective parameters, we newly demonstrate that iPS cell colony possess particular morphological character

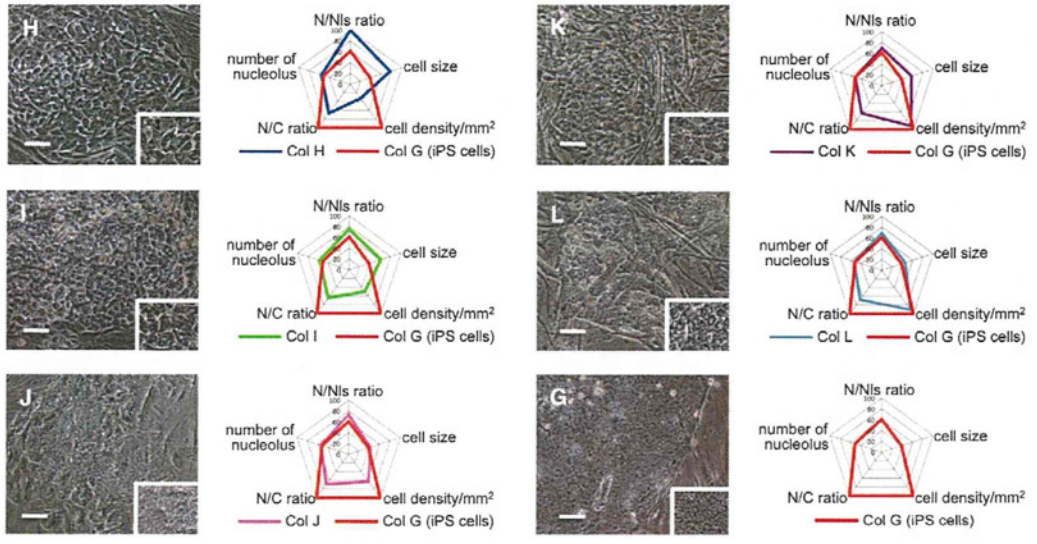

Figure 4. Morphometric analysis in colonies generated from human fibroblasts by using a single polycistronic Oct3/4-Klf4-Sox2-c-Myc-GFP expressing viral vector. (H–L, G) Photograph and parameters of colonies H~L and G. Graphs shows parameters of each classified colony, including that of iPS cell colony G. The numerical value in the graph indicate the ratio to the maximum value (setting 100 for maximum value) in each parameter. Scale bars = 100 μm.
doi:10.1371/journal.pone.0048677.g004

compared to non-iPS cell colonies in that iPS cells show maximum value in cell density and N/C ratio and minimum in cell size, number of nucleoli and N/Nls ratio. In addition, iPS cell colony can be specifically identified by their expression of Sox2 and Cdx2. Thus, both morphologic features and expression both of Cdx2 and Sox2 would improve the precision of iPS cell generation ratio. However, Sox2 is reported to be expressed in neural stem cells or other tissue stem cells [20,21,22]. Therefore, in the case of generating iPS cells from stem cells that already express endogenous Sox2, Cdx2 expression and morphologic parameters will be helpful for iPS cell identification. In addition, since Cdx2 is not expressed in human ES cells, this gene is considered specific for iPS cells. The function of Cdx2 in iPS cells need to be clarified in the future.

Previous studies reported gene expression analyses that were performed using live cell imaging and Q-PCR in both ES-like and non-ES like colonies [6,23]. In these reports, Nanog, Oct3/4, and alkaline phosphatase were expressed in various types of colonies and considered to be inadequate markers to identify iPS cells [6,23]. In this study, however, we showed that colonies other than iPS cells express both Nanog and endogenous Oct3/4, and therefore iPS cell identification based on Nanog or Oct3/4 is not reliable method. Furthermore, that may contaminate non-iPS cells into iPS cell count, leading to the overestimation of iPS cell generation ratio.

Up to now, iPS cell generation efficiency was often calculated based on the expression of reporter genes such as GFP under the control of certain gene promoters [8,9]. However, none of the studies examined whether the expression of these reporter genes are truly appropriate to identify iPS cells. At least in the case of Nanog and Oct3/4, our result suggested that the expression of these reporter genes is not reliable for identification of iPS cells. Furthermore, it is reported that the expression of reporter gene under the control of specific gene promoter do not reflect the true expression of the specific gene in some cases [24,25]. In this sense, whether the reporter gene under the control of Cdx2 appropriately function for iPS cell generation needs to be clarified in the future.

Objective criteria for identifying iPS cells have not yet been established. Selecting iPS cells or calculating the iPS cell generation ratio using accurate and objective method is necessary for standardization of iPS cell research, and, from this viewpoint our results will contribute to the establishment of unified criteria for objectively identifying iPS cells.

Materials and Methods

Ethics Statement

All animal experiments were approved by the Animal Care and Experimentation Committee of Tohoku University Graduate School of Medicine. The entire study was conducted in accordance with the Declaration of Helsinki. Human ES cell line Kyoto hESC-1 was obtained from the Institute for Frontier Medical Science of Kyoto University (Japan) with approval for hESC use granted by the Ministry of Education, Culture, Sports, Science, and Technology of Japan.

Gene introduction and iPS cell generation

Normal human dermal fibroblasts were obtained from Lonza (Basel, Switzerland). Cells were cultured in alpha-minimum Essential Medium Eagle Modification (Sigma, St. Louis, MO) containing 10% fetal bovine serum and 0.1 mg/ml kanamycin at 37°C and 5% CO_2. Induced pluripotent stem cells were generated as reported by Takahashi et al [3]. The open reading frames of human Oct3/4, Sox2, Klf4, and c-Myc were amplified by RT-PCR using PrimeSTAR HS DNA Polymerase (TaKaRa, Shiga, Japan) and inserted into pMXs retroviral vectors. These plasmids were transfected into PLAT-A retroviral packaging cells followed by incubation in Dulbecco's Modified Eagle Medium containing 10% fetal bovine serum. Forty-eight hours after transfection, the viral supernatant was collected and filtered through a 0.45-μm filter. The virus-containing flow-through was concentrated by centrifugation at 8000× g for 16 h at 4°C.

Table 2. Classification of morphologic characteristics in colonies generated from human fibroblasts using a single polycistronic viral vector.

	number of nucleolus	nucleus to nucleolus ratio	cell size	cell density/mm^2	nucleus to cytoplasm ratio	number of layer	number of colonies obtained (Experiment 1)	number of colonies obtained (Experiment 2)
Col H	1.30±0.50	3.60±0.60	87.50±9.36	1933.34±19.05	0.58±0.06	single	16	11
Col I	1.33±0.54	2.71±0.46	70.01±7.13	2962.96±20.91	0.56±0.05	single	64	66
Col J	1.26±0.47	2.65±0.45	47.09±7.34	3745.00±24.86	0.61±0.07	multilayer	71	69
Col K	1.20±0.45	2.50±0.49	65.06±5.69	5466.67±40.92	0.55±0.05	single	16	23
Col L	1.25±0.47	2.48±0.39	51.55±5.91	5383.84±34.67	0.59±0.06	multilayer	30	21
Col G (iPS cell)	1.20±0.45	2.19±0.17	43.50±2.96	5933.33±20.82	0.87±0.04	single	2	2

Each replicate represented 2×10^5 GFP positive cells seeded onto a 60-mm dish containing feeder cells and cultured in Primate ES cell medium for thirty days.
doi:10.1371/journal.pone.0048677.t002

For iPS cell generation, human fibroblasts were seeded at 2×10^5 cells in a 60-mm dish. The next day, concentrated virus plus 4 μg/ml Polybrene (Nacalai Tesque, Kyoto, Japan) was added to the medium. Twenty-four hours after transduction, the virus-containing medium was replaced with new medium without virus. After 5 days, fibroblasts were trypsinized and 1×10^5 cells were transferred onto inactivated mouse embryonic fibroblasts cultured in a 100-mm diameter dish. The next day, the medium was replaced with Primate ES cell medium (ReproCELL, Kanagawa, Japan) supplemented with 4 ng/ml basic fibroblast growth factor (Peprotech, Rock Hill, NJ). The medium was changed every other day. Thirty-five days after transduction, all colonies were picked and individually transferred onto inactivated mouse embryonic fibroblasts in 4-well plates. Detailed information for the single polycistronic retroviral vector encoding the four transcription factors was described in a previous report [10].

Statistical analysis

Morphometric data of randomly selected five cells from the central region of each generated colony are analyzed and presented as the mean ± s.d. Cell density and cell size were analyzed by t-test with Bonferroni's correction for multiple comparisons. Number of nucleoli and the N/C and N/Nls ratios were analyzed using the Chi-square test and Mann-Whitney U test, respectively, both with Bonferroni's correction. In the Bonferroni's correction, the actual level of significance was corrected to and accepted as $p<0.01$ to correct for the five pairwise comparisons.

RNA extraction and RT-PCR

Three individual colonies were randomly selected from each colony subtype and subjected to RT-PCR. Total RNA was purified with an RNeasy Mini Kit (QIAGEN, Hilden, Germany). RNA (500 ng) was reverse-transcribed using a SuperScript VILO cDNA Synthesis Kit (Invitrogen, Carlsbad, CA) according to the manufacturer's instructions. The PCR reactions were performed using Ex Taq DNA Polymerase (TaKaRa). The primer set for a pluripotency marker FoxD3 was:

sense, 5′- CTGCCTCTCCCCAATTTCCT-3′ and antisense, 5′- TCCCATCCCCACGGTACTAA -3′.The RT-PCR primer sets for the other genes were described previously [10]. The primer sets for Oct3/4 and Sox2 were designed from the untranslated region, which does not detect the retroviral transcripts, so that the primers specifically detect the transcripts from the endogenous Oct3/4 and Sox2 genes.

The signal intensity for each factor occasionally differed among colonies, but the gene expression pattern was same among colonies that belong to the same subtype. Therefore, one colony was randomly selected from each colony subtype and demonstrated in figure 1H.

Q-PCR

Three individual colonies were randomly selected from each colony subtype and subjected to Q-PCR. cDNA was synthesized using a High Capacity cDNA Reverse Transcription Kit (Applied Biosystems, Foster, CA). After cDNA preparation, genes of interest were amplified using TaqMan gene expression assays (Applied Biosystems). Q-PCR was performed with a 7300 real-time PCR system (Applied Biosystems) using the following PCR primer sets, Oct3/4 (Hs03005111_g1), Sox2 (Hs01053049_s1), Nanog (Hs02387400_g1), Klf4 (Hs00358836_m1), c-Myc (Hs99999003_m1), FoxD3 (Hs00255287_s1), Rex1 (Hs00399279_m1), Dnmt3b (Hs00171876_m1), Abcg2

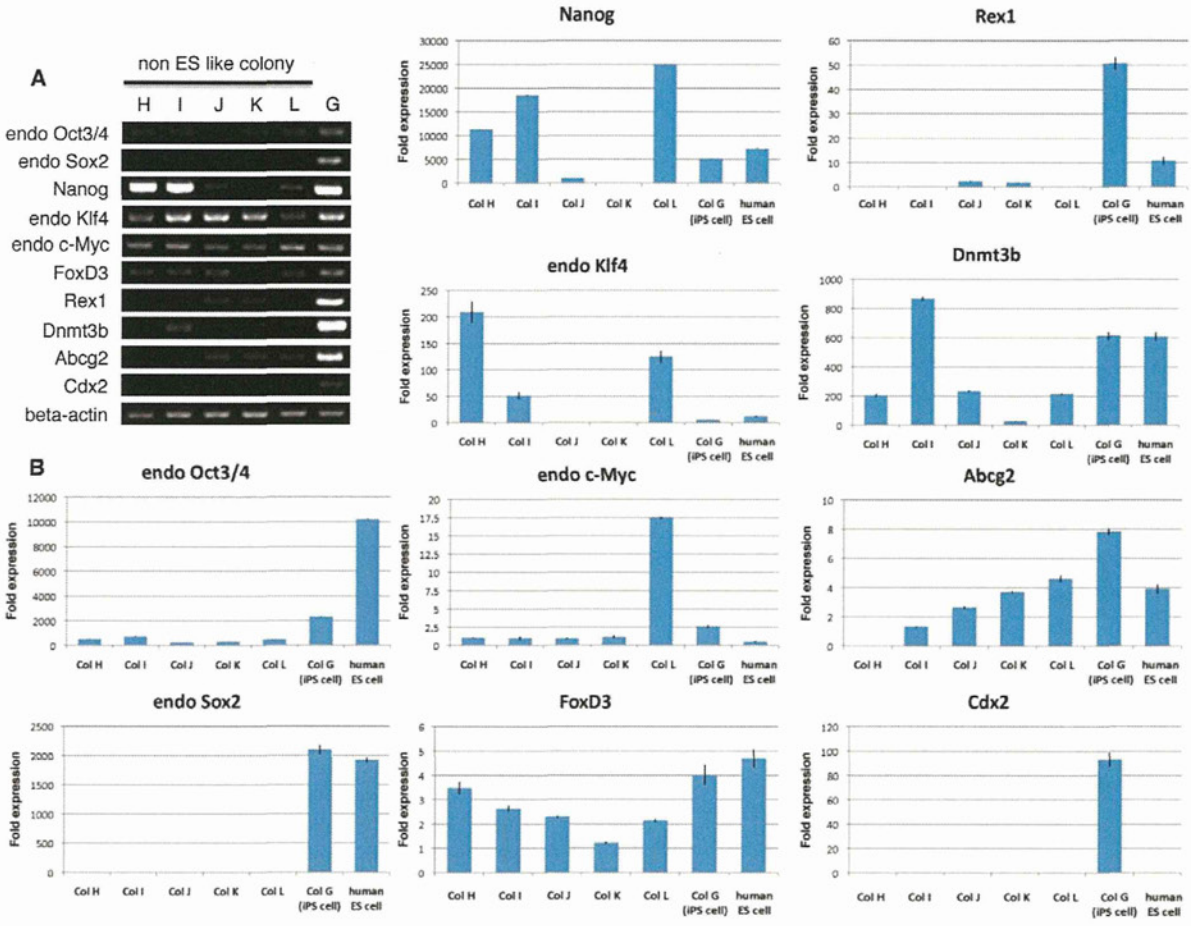

Figure 5. RT-PCR and Q-PCR of typical examples in each colonies H~L and iPS colony G and human ES cells. (A) RT-PCR analysis examined the expression of endogenous Oct3/4, Sox2, Nanog, Klf4, c-Myc, as well as FoxD3, Rex1, Dnmt3b, Abcg2 and Cdx2. Beta-actin was used as an internal control. (B) Q-PCR data for expression of endogenous Oct3/4, endogenous Sox2, Nanog, endogenous Klf4, endogenous c-Myc, FoxD3, Rex1, Dnmt3b, Abcg2 and Cdx2.
doi:10.1371/journal.pone.0048677.g005

(Hs01053790_m1), Cdx2 (Hs01078080_m1) and beta-actin (Hs99999903_m1). Data were processed using the ΔΔCt method.

EBs formation from iPS cells and non-ES like colonies

iPS cells and non-ES like colonies were harvested by mechanical pick-up. The clumps of cells were transferred to poly 2-hydroxyethyl methacrylate-coated dish in Dulbecco's Modified Eagle Medium/F12 containing 20% knockout serum replacement (Invitrogen), 1×10^{-4} M nonessential amino acids, 1×10^{-4} M 2-mercaptoethanol, 2 mM L-glutamine, and 0.1 mg/ml kanamycin. The medium was changed every other day. After 10 days, EBs were transferred to gelatin-coated plates and cultured in the same medium for another 10 days.

Teratoma formation

iPS cells were suspended at 1×10^7 cells in 0.02 M PBS and were injected using glass microtubes into the testes of 8 weeks old NOG mice [NOD/Shi-scid [26] IL-2RγKO Jic mice; ICLAS Monitoring Center, Japan]. As negative control, testes were injected with mouse embryonic fibroblasts treated with mitomycin C. 12 weeks after injection, all mice were killed and fixed with 4% PFA in 0.1 M PBS. These fixed testes were embedded in paraffin, and cut into sections 10 μm thick. These sections were stained with hematoxylin and eosin.

Supporting Information

Figure S1 *In vitro* embryoid body (EB) formation. (**A**) EBs generated in suspension culture from iPS cell colony G. (B) Cell clusters generated in suspension from colony C as representative of colonies A~F. Scale bars = 100 μm.
(TIF)

Author Contributions

Conceived and designed the experiments: SW MK MD. Performed the experiments: SW YK FO TM. Analyzed the data: SW MK MD. Contributed reagents/materials/analysis tools: SW YK FO TM AN. Wrote the paper: MD MK SW.

References

1. Thomson JA, Itskovitz-Eldor J, Shapiro SS, Waknitz MA, Swiergiel J, et al. (1998) Embryonic stem cell lines derived from human blastocysts. Science. 282, 1145–1147.
2. Cowan CA, Klimanskaya I, McMahon J, Atienza J, Witmyer J, et al. (2004) Derivation of embryonic stem-cell lines from human blastocysts. N Engl J Med.350, 1353–1356.
3. Takahashi K, Tanabe K, Ohnuki M, Narita M, Ichisaka T, et al. (2007) Induction of pluripotent stem cells from adult human fibroblasts by defined factors. Cell.131, 861–872.
4. Dimos JT, Rodolfa KT, Niakan KK, Weisenthal LM, Mitsumono H, et al. (2008) Induced pluripotent stem cells generated from patients with ALS can be differentiated into motor neurons. Science. 321, 1218–1221.
5. Ebert AD, Yu J, Rose FFJr, Mattis VB, Lorson CL, et al. (2009) Induced pluripotent stem cells from a spinal muscular atrophy patient. Nature. 457, 277–280.
6. Masaki H, Ishikawa T, Takahashi S, Okumura M, Sakai N, et al. (2007) Heterogeneity of pluripotent marker gene expression in colonies generated in human iPS cell induction culture. Stem Cell Res. 1, 105–115.
7. Huangfu D, Maehr R, Guo W, Eijkelenboom A, Snitow M, et al. (2008) Induction of pluripotent stem cells by defined factors is greatly improved by small-molecule compounds. Nat Biotechnol. 26, 795–797.
8. Wernig M, Meissner A, Foreman R, Brambrink T, Ku M, et al. (2007) *In vitro* reprogramming of fibroblasts into a pluripotent ES-cell-like state. Nature. 448, 318–324.
9. Okita K, Ichisaka T. Yamanaka S (2007) Generation of germline-competent induced pluripotent stem cells. Nature. 448, 313–317.
10. Wakao S, Kitada M, Kuroda Y, Shigemoto T, Matsuse D, et al. (2011) Multilineage-differentiating stress-enduring (Muse) cells are a primary source of induced pluripotent stem cells in human fibroblasts. Proc. Natl. Acad. Sci. USA. 108, :9875–9880.
11. International Stem Cell Initiative, Adewumi O, Aflatoonian B, Ahrlund-Richter L, Amit M, et al. (2007) Characterization of human embryonic stem cell lines by the International Stem Cell Initiative. Nat. Biotechnol. 25, 803–816.
12. Brimble SN, Zeng X, Weiler DA, Luo Y, Liu Y, et al. (2004) Karyotypic stability, genotyping, differentiation, feeder-free maintenance, and gene expression sampling in three human embryonic stem cell lines derived prior to August 9, Stem Cells Dev. 13, 585–597.
13. Sperger JM, Chen X, Draper JS, Antosiewicz JE, Chon CH, et al. (2003) Gene expression patterns in human embryonic stem cells and human pluripotent germ cell tumors. Proc. Natl. Acad. Sci. USA 100, 13350–13355.
14. Ware CB, Nelson AM. Blau CA (2006) A comparison of NIH-approved human ESC lines. Stem Cells. 24, 2677–2684.
15. Chambers I, Colby D, Robertson M, Nicols J, Lee S, et al. (2003) Functional expression cloning of Nanog, a pluripotency sustaining factor in embryonic stem cells. Cell. 113, 643–655.
16. Niwa H, Miyazaki J, Smith AG (2000) Quantitative expression of Oct-3/4 defines differentiation, dedifferentiation or self-renewal of ES cells. Nat. Genet. 24, 372–376.
17. Masui S, Nakatake Y, Toyooka Y, Shimosato D, Yagi R, et al. (2007) Pluripotency governed by Sox2 via regulation of Oct3/4 expression in mouse embryonic stem cells. Nat. Cell Biol. 9, 625–635.
18. Adachi K, Suemori H, Yasuda SY, Nakatsuji N, Kawase E (2010) Role of SOX2 in maintaining pliripotency of human embryonic stem cells. Genes Cells. 15: 455–470
19. Khoo ML, McQuade LR, Smith MS, Lees JG, Sidhu KS, et al. (2005) Growth and differentiation of embryoid bodies derived from human embryonic stem cells: effect of glucose and basic fibroblast growth factor. Biol. Reprod. 73, 1147–1156.
20. Zappone MV, Galli R, Catena R, Meani N, De Biasi S, et al. (2000) Sox2 regulatory sequences direct expression of a b-geo transgene to telencephalic neural stem cells and precursors of the mouse embryo, revealing regionalization of gene expression in CNS stem cells. Development. 127:2367–82.
21. Biernaskie J, Paris M, Morozova O, Fagan BM, Marra M, et al. (2009) SKPs Derive from Hair Follicle Precursors and Exhibit Properties of Adult Dermal Stem Cells. Cell Stem Cell. 5:610–623.
22. Kuroda Y, Kitada M, Wakao S, Nishikawa K, Tanimura Y, et al. (2010). Unique multipotent cells in adult human mesenchymal cell populations. Proc Natl Acad Sci U S A. 107:8639–8643.
23. Chan EM, Ratanasirintrawoot S, Park IH, Manos PD, Loh YH, et al. (2009) Live cell imaging distinguishes bona fide human iPS cells from partially reprogrammed cells. Nat. Biotechnol. 27, 1033–1037.
24. Spassky N, Goujet-Zalc C, Parmantier E, Olivier C, Martinez S, et al. (1998) Multiple restricted origin of oligodendrocytes. J Neurosci. 18:8331–8343.
25. Spassky N, Olivier C, Perez-Villegas E, Goujet-Zalc C, Martinez S, et al. (2000) Single or multiple oligodendroglial lineages: a controversy. Glia. 29:143–148.
26. Ito M, Hiramatsu H, Kobayashi K, Suzue K, Kawahata M, et al. (2002) NOD/SCID/gamma(c)(null) mouse: an excellent recipient mouse model for engraftment of human cells. Blood. 1: 3175–3182.

Cells **2012**, *1*, 1045-1060; doi:10.3390/cells1041045

OPEN ACCESS

cells

ISSN 2073-4409

www.mdpi.com/journal/cells

Review

Regenerative Effects of Mesenchymal Stem Cells: Contribution of Muse Cells, a Novel Pluripotent Stem Cell Type that Resides in Mesenchymal Cells

Shohei Wakao [1], Yasumasa Kuroda [2], Fumitaka Ogura [1], Taeko Shigemoto [1] and Mari Dezawa [1,2,*]

[1] Department of Stem Cell Biology and Histology, Tohoku University Graduate School of Medicine, Sendai, 980-8575, Japan; E-Mails: wakao@med.tohoku.ac.jp (S.W.); f.ogura@med.tohoku.ac.jp (F.O.); tshigemoto@med.tohoku.ac.jp (T.S.)

[2] Department of Anatomy and Anthropology, Tohoku University Graduate School of Medicine, Sendai, 980-8575, Japan; E-Mail: y-kuroda@med.tohoku.ac.jp

* Author to whom correspondence should be addressed; E-Mail: mdezawa@med.tohoku.ac.jp; Tel: +81-22-717-8025.

Received: 8 October 2012; in revised form: 1 November 2012 / Accepted: 5 November 2012 / Published: 8 November 2012

Abstract: Mesenchymal stem cells (MSCs) are easily accessible and safe for regenerative medicine. MSCs exert trophic, immunomodulatory, anti-apoptotic, and tissue regeneration effects in a variety of tissues and organs, but their entity remains an enigma. Because MSCs are generally harvested from mesenchymal tissues, such as bone marrow, adipose tissue, or umbilical cord as adherent cells, MSCs comprise crude cell populations and are heterogeneous. The specific cells responsible for each effect have not been clarified. The most interesting property of MSCs is that, despite being adult stem cells that belong to the mesenchymal tissue lineage, they are able to differentiate into a broad spectrum of cells beyond the boundary of mesodermal lineage cells into ectodermal or endodermal lineages, and repair tissues. The broad spectrum of differentiation ability and tissue-repairing effects of MSCs might be mediated in part by the presence of a novel pluripotent stem cell type recently found in adult human mesenchymal tissues, termed multilineage-differentiating stress enduring (Muse) cells. Here we review recently updated studies of the regenerative effects of MSCs and discuss their potential in regenerative medicine.

Keywords: pluripotent stem cells; mesenchymal stem cells; transdifferentiation; tissue repair; cell therapy

1. Introduction

Mesenchymal stem cells (MSCs) are cells that reside in tissues such as bone marrow, fat tissue, dermis, and the umbilical cord, and are useful for cell-based therapy in humans because of their low risk of tumorigenesis [1,2]. MSCs have pleiotropic actions; not only do they exert trophic and anti-inflammatory effects on damaged tissues by producing a variety of trophic factors and cytokines, but they also modulate immunologic reactions, which is the basis for their application in graft-versus-host disease [3–5].

Besides the mechanisms underlying the trophic, anti-inflammatory, and immunomodulatory effects, another important action of MSCs that has been debated over the past decade is the broad spectrum of differentiation beyond the boundaries of tissue stem cells. Generally, tissue stem cells generate the cell types of the tissue in which they reside, and thus the range of their differentiation capabilities is usually limited. For example, hematopoietic stem cells generate blood cells and neural stem cells generate neurons, astrocytes, and oligodendrocytes [6,7]. MSCs belong to the mesodermal lineage, so it would be reasonable that they differentiate into cells of the same mesodermal lineage, such as osteocytes, cartilage cells, and adipocytes [8–11], and other mesodermal lineage cells, such as skeletal muscle cells, endothelial cells, and cardiomyocytes [8–11]. Interestingly, however, MSCs also differentiate into the other lineages, endodermal and ectodermal cells, such as hepatocytes, insulin-producing cells, neuronal cells, and peripheral glial cells [12–16]. Such a broad spectrum of differentiation has been observed in *in vitro* experiments using cytokine induction and/or gene introduction. MSCs also spontaneously differentiate into mesodermal, ectodermal, or endodermal cells with a very low frequency *in vivo*. When transplanted, these cells home to the damaged site and differentiate into cardiomyocytes (mesodermal), hepatocytes (endodermal), and keratinocytes (ectodermal) according to the local microenvironment they integrated and contribute to tissue repair [17–19].

Based on these reports, it has been speculated that MSCs contain cells resembling pluripotent stem cells that also work as 'repair cells' *in vivo*, but because of a lower ratio of triploblastic differentiation, such putative cells are considered to comprise a very small subpopulation of MSCs. Recently, adult human mesenchymal cells have been reported to contain a novel type of pluripotent stem cell population that may explain the triploblastic differentiation and tissue repair effect observed in MSCs [20]. In this review, the unique properties of MSCs and their great possibility for regenerative medicine are discussed.

2. MSC Heterogeneity

MSCs are usually harvested just as adherent cells from mesenchymal tissues, such as the dermis, bone marrow, adipose tissue, and umbilical cord. Due to this unsophisticated simple method of collection, MSCs are seen as crude cell populations comprising a heterogeneous population. The individual populations comprising mesenchymal cells often differ with regard to origin, phenotype, and differentiation state [21]. For simplicity, however, such crude cells are called MSCs, even though a robust characterization of their stemness is lacking.

Dermal fibroblasts are one type of the MSCs that are usually collected from adherent dermal cell cultures, but the so-called fibroblasts are not a single cell population because the dermis comprises various cell types, such as fibroblasts (the major component of the connective tissue), blood

vessel-associated cells (endothelial cells and pericytes), sensory nerve-related glial cells (Schwann cells), as well as several types of stem or progenitor cells, such as skin-derived precursors, neural crest-derived stem cells, melanoblasts, perivascular cells, endothelial progenitors, and adipose-derived stem cells [22–29]. In fact, primary cultured dermal cells contain cells positive for CD117 (a marker for melanoblasts), CD146 (perivascular cells and adipose-derived stem cells), CD271 (neural crest-derived stem cells), Snail (skin-derived precursors), and Slug (skin-derived precursors) [3].

This cell population heterogeneity is also found in another mesenchymal cell type, bone marrow-derived mesenchymal cells. These cells are often called bone marrow MSCs (BM-MSCs) and are also usually collected as adherent cells from bone marrow aspirates and are thus heterogeneous. As reported by Pittenger *et al.* [8], BM-MSCs are positive for mesenchymal markers, but the marker content and expression ratios differ among batches.

The definition of a 'stem cell' requires that the cells possess two properties, self-renewal (the ability to renew themselves through mitotic cell division) and potency (ability to differentiate into a diverse range of specialized cell types) [30]. Potency specifies the differentiation potential of the stem cell; pluripotent stem cells are defined as cells that can differentiate into cells of either ectodermal, endodermal, or mesodermal lineage, and multipotent stem cells are defined as those that can differentiate into a number of cells, mostly those of a related family of cells that belong to the same cell lineage such as in the case of differentiation of MSCs into osteocytes, adipocytes, and chondrocytes [30]. To be precise, stem cells must meet these requirements at a single cell level, as seen in the characterization of neural stem cells: sphere formation and differentiation into neurons and glial cells. In the case of MSCs, however, the heterogeneity makes it difficult to appropriately verify putative rare pluripotent stem cells that might be responsible for triploblastic differentiation. From that standpoint, the differentiation ability of MSCs has remained an enigma.

3. Controversy over Pluripotency of Mesenchymal Cells

Over the past decade, it has been argued whether MSCs could have pluripotency characteristics. Verfaillie *et al.* described that MSCs derived from adult bone marrow, which they named multipotent adult progenitor cells (MAPC). MAPCs could also be considered a pluripotent stem cell type because they can be differentiated into cells representative of all three germ layers [31]. Because other laboratories have not been able to produce MAPCs, however, their existence has been questioned. Ratajczak *et al.* reported that a population of very small embryonic-like cells, named VSEL cells, expressing the known embryonic stem (ES) cell markers Oct-4, Nanog, and Rex-1, are able to differentiate into cardiac (mesodermal), neural (ectodermal), and pancreatic (endodermal) cells and therefore are pluripotent stem cells [32], but the existence of VSEL cells has also recently been questioned by another group [33]. While the reports of pluripotent cells are exciting and suggest the potential pluripotency of MSCs, their existence is uncertain due to insufficient identification of specific convincing markers for MAPCs or VSEL cells and the lack of reproducibility between different labs.

As mentioned above, the definition of 'pluripotent stem cells' applies both to triploblastic differentiation and self-renewal. In addition to the above two properties that mimic normal development, however, definition of pluripotency often includes germ line-transmitting chimeras

and/or teratomas [30,34]. This is typically observed with ES cells and induced pluripotent stem (iPS) cells, while another type of pluripotent stem cell type, epiblast stem cells, does not form teratomas under certain circumstances [35].

The argument of MSC pluripotency has been argued because MSC do not produce the germ line-transmitting chimeras and/or teratomas in question. MSCs indeed show triploblastic differentiation both *in vitro* and *in vivo*, and in this regard they are often called pluripotent. MSCs do not contribute to teratoma formation nor germ line transmitting chimeras, however, and thus MSCs are sometimes described as 'multipotent' and not pluripotent [8]. It is understandable that MSCs, which normally reside in mesenchymal tissues, are not tumorigenic and thus do not from teratomas when transplanted *in vivo*. There may be fundamental differences between MSCs and cells that contribute to germ line-transmitting chimeras, such as ES cells. The term 'multipotency', however, may not be adequate to describe their triploblastic differentiation ability. Overall, 'self-renewal' and 'triploblastic differentiation' could be considered essential and common requirements for all kinds of pluripotent stem cells, and these two properties are sufficiently comprehensive and practical to represent the high differentiation ability of MSCs rather than setting limits by including generation of germ line-transmitting chimeras and/or teratoma formation abilities. More importantly, if cells that are pluripotent but do not form tumors can be obtained from normal human tissues, this will be beneficial for cell-based therapy.

4. Mesenchymal Cells Contain Pluripotent Stem Cells

A novel pluripotent stem cell type, multilineage-differentiating stress enduring (Muse) cells, has recently been identified in adult human mesenchymal tissues [20]. Muse cells are unique because they show pluripotency aspects such as the expression of pluripotency markers, self-renewal ability and triploblastic differentiation, while at the same time they also demonstrate the characteristics of mesenchymal cells [20]. In other words, they are double-edged, both pluripotent and mesenchymal cell-like.

Muse cells were found initially as stress-tolerant cells [20]. Tissue stem cells are normally dormant and not active, but once the tissue is damaged or exposed to stress, they are activated to start proliferating, differentiating, and contributing to tissue repair. For example, neural stem cells that are located in the brain are normally inactive, but following stroke, those stem cells enter into the cell cycle and generate neural cells, including neurons [36]. Muse cells are a kind of stem cell that is stress tolerant.

When mesenchymal cells, such as human BM-MSCs or dermal fibroblasts, are cultured for longer than overnight under stress-inducing conditions, *i.e.*, trypsin incubation or low nutrition, the large majority of mesenchymal cells dies out and only a small number of cells survive. When those surviving cells are cultured in a single cell-suspension culture, they form clusters that are very similar to the embryoid bodies formed by human ES cells that express pluripotency markers, show triploblastic differentiation, and self-renewal ability (Figure 1). To collectively represent the properties of those cells, they were named multilineage-differentiating stress enduring cells [20].

Figure 1. Isolation and characterization of Muse cells.

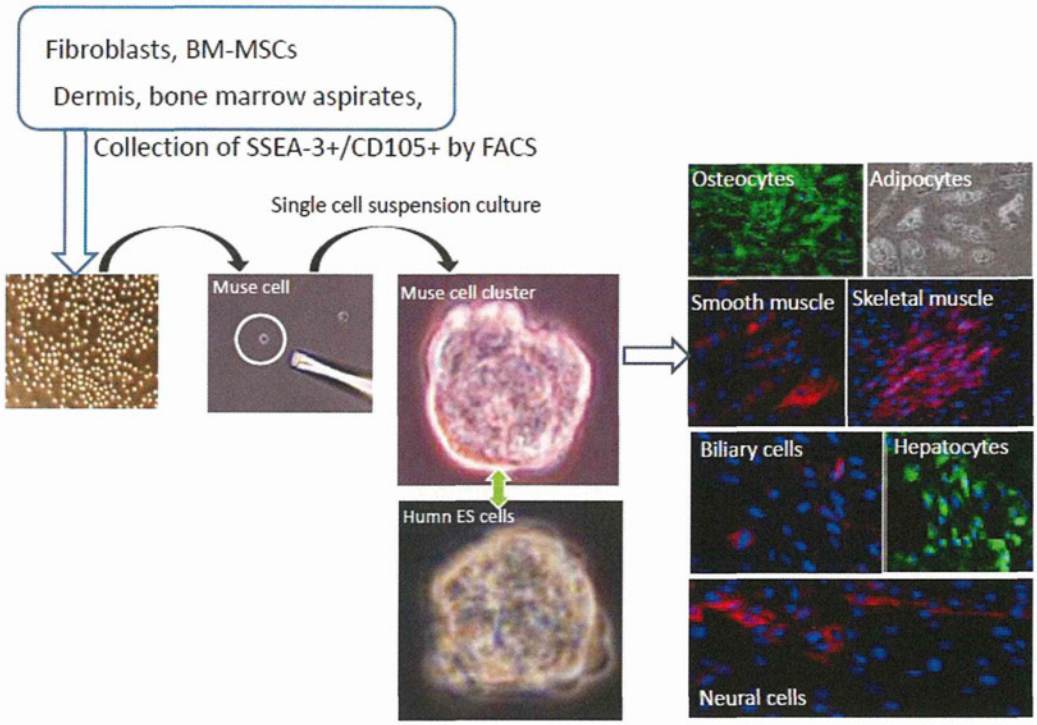

Muse cells can be collected from cultured mesenchymal cells (fibroblasts or BM-MSCs) and mesenchymal tissues (dermis, and bone marrow aspirates) as cells double positive for SSEA-3 and CD105. Collected Muse cells express SSEA-3 on their surface, similar to human embryonic stem (ES) cells. After isolating Muse cells by fluorescence-activated cell sorting, single Muse cells cultured in suspension (single cell-suspension culture) generate characteristic clusters that are very similar to the embryoid bodies formed by human ES cells. When the cell clusters are transferred onto gelatin culture and spontaneous differentiation is induced, cells with endodermal- (hepatocytes; α-fetoprotein+ and biliary cells; cytokeratin7+), ectodermal- (neuronal cells; neurofilament+), and mesodermal- (osteocytes; osteocalcin+, adipocytes; lipid droplets+, smooth muscle cells; smooth muscle actin+, skeletal muscle cells; desmin+) lineage are observed. (See Figure 1, pictures adapted with permission from Y. Kuroda *et al.* (2010). 2010 The National Academy of Science, and with permission from Wakao *et al.* (2011). 2011 The National Academy of Science.) [3,20].

A specific marker for Muse cells was investigated by comparing the expression pattern of cells before and after long-term stress incubation. Among many candidate cell surface markers, a positive ratio for SSEA-3, a well-known marker for undifferentiated human ES cells, drastically increases after stress incubation. When human fibroblasts and BM-MSCs are separated into SSEA-3-positive and SSEA-3-negative populations and subjected to single cell-suspension culture, only the SSEA-3 positive cells generate the clusters mentioned above, indicating that Muse cells are SSEA-3-positive cells [20]. Muse cells are further clarified to express mesenchymal markers, such as CD29, CD90, and CD105, so that Muse cells can be identified as cells double-positive for mesenchymal and pluripotency markers (Figure 1) [3].

Muse cells are double-edged, not only in the uniqueness of their surface marker expression profile, but also in their behavior and other properties. In adherent culture, they appear the same as the general

population of mesenchymal cells, such as fibroblasts, but when they are transferred to a single cell-suspension culture, the cells proliferate and form cell clusters that resemble ES embryoid bodies (Figure 1). Such single cell-derived Muse cell clusters are not only similar to pluripotent stem cells like ES cells in their appearance, but also in their positivity for alkaline phosphatase as well as for the pluripotency markers Nanog, Oct3/4, and Sox2. Most importantly, they differentiate into endodermal-, ectodermal-, and mesodermal-lineage cells when transferred to gelatin cultures, indicating that single Muse cells are able to generate cells representative of all three germ layers (Figure 1). Muse cells are also able to self-renew while maintaining a normal karyotype [3,20].

As mentioned above, the existence of pluripotent cells in MSCs has long been suggested, but to date there have been no reports clearly demonstrating self-renewal and triploblastic differentiation at a single cell level, so the pluripotency among MSCs remained controversial [37,38]. Most importantly, single Muse cells are able to generate osteocytes, adipocytes, chondrocytes, skeletal muscle cells, smooth muscle cells (mesodermal-lineage); neuronal cells, epidermal cells (ectodermal-lineage); and hepatocytes, and biliary cells (endodermal-lineage cells) *in vitro*, and keep self-renewing, so that they are considered pluripotent stem cells (Figure 1). When Muse cells spontaneously differentiate (*i.e.*, without trophic factors), the mesodermal-lineage differentiation percentage is slightly higher (10%~15%) than ectodermal (3%~4%) or endodermal (3%~4%)-lineage-differentiated cells that cross over the oligolineage boundaries between germ layers [3,20].

5. Muse Cells Are Directly Reprogrammed into Desired Cells by Induction

While Muse cells spontaneously differentiate into mesodermal-, ectodermal-, and endodermal-lineage cells, their differentiation ratio is not very high. When Muse cells are treated with a certain combination of cytokines and trophic factors, more than 90% of the cells can be directed to differentiate into purposive cells. For example, when Muse cells are treated with hepatocyte growth factor, fibroblast growth factor 4, and dexamethasone in insulin-transferrin-selenite medium, ~90% of the cells become positive for alpha-fetoprotein and human albumin, hepatocyte markers, within 4 weeks. Similarly, ~90% of Muse cells treated with Neurobasal medium with B-27 supplement, basic fibroblast growth factor, and EGF differentiate into MAP-2- or neurofilament-positive cells by neuronal induction; namely, generating neurospheres, followed by differentiation into neuronal cells when treated with basic fibroblast growth factor and brain-derived neurotrophic factor. In osteocyte or adipocyte induction medium, ~98% of Muse cells differentiate into cells positive for osteocalcin or oil-red, respectively. In this manner, desired cells either of mesodermal-, ectodermal- or endodermal-lineage cells can be efficiently obtained from Muse cells depending on the induction treatment. More importantly, none of the above-mentioned differentiations require the introduction of exogenous genes, so that Muse cells produce the desired cells with lower risks [3].

6. Muse Cells are Different from Known Stem Cells in the Mesenchymal Tissues, Dermis, and Bone Marrow

While Muse cells are found in the bone marrow and dermis, these tissues also contain several kinds of stem cells. Bone marrow contains several stem cell types, including BM-MSCs, hematopoietic lineage cells, and endothelial cells [19]. To determine the localization of Muse cells within these